Spectral decomposition of the perturbation response of the Schwarzschild geometry

Edward W. Leaver*
Department of Physics and The College of Science Computer, University of Utah, Salt Lake City, Utah 84112
(Received 10 February 1986)

The radiative Green's function for the one-dimensional wave equation with the Regge-Wheeler and Zerilli potentials is formally constructed from recently developed analytic representations for generalized spheroidal wave functions, and decomposed into a convergent sum over quasinormal modes, an integral around a branch cut in the frequency domain, and a high-frequency remnant of the free-space propagator. This paper discusses the contribution to the time response made by the quasinormal modes and, at very late times, by the branch-cut integral. The initial-value problem is considered for source fields with both compact and extended radial dependences, and the problem of the formal divergence of the integrals of extended sources over quasinormal-mode wave functions is solved. The branch-cut integral produces a weak late-time radiative power-law decay tail that will characterize the astrophysically observed radiation spectrum for times subsequent to the exponential decay of the quasinormal ringing, when $(ct-r_*)\gg 2MG/c^2$ and $(ct-r_*)/r_* \ll 1$. This radiative decay tail is shown to diminish to Price's nonradiative tail in the final limit $ct/r_* \gg 1$. The method is applied to a characteristic-value problem used to model the gravitational collapse of massive stars, and to the small-body radial in-fall problem. The analysis presented is generalizable, through the Newman-Penrose formalism and Teukolsky's equations, to obtain the radiative Green's function for perturbations to the Kerr geometry.

I. INTRODUCTION

Although Green's-function techniques have for many years been used to describe radiation phenomena involving perturbations to black-hole geometries,[1-5] the relevant wave equations have thus far been integrable only by numerical methods, and no analytic insight has been afforded into the nature of the propagator function itself. The present study uses new results concerning generalized spheroidal wave functions to describe some of the analytic properties of the radiative Green's function that propagates small perturbations to the Schwarzschild geometry. While the Schwarzschild geometry itself is of diminishing interest in studies of black-hole dynamics, as current questions concerning black-hole stability and radiance focus on rotating and charged black holes, there remain a few outstanding questions concerning the physical significance of the resonant, or quasinormal, modes of any black hole. In particular, while a quasinormal-mode decomposition, or singularity expansion, seems a desirable approach to the interpretation of gravitational radiation expected from (for instance) type-II supernova in terms of stellar conditions prevalent at the final stage of the collapse, formal divergence of the integrals describing the excitation of the quasinormal ringing, a paucity of values for all but the least damped of the quasinormal frequencies, lack of analytic representation for the quasinormal-mode wave functions, and the question of the relative completeness of the quasinormal modes, have heretofore made the interpretation of proposed quasinormal mode decompositions impossible. The present analysis addresses these questions, and the relative familiarity of most properties of the Schwarzschild geometry allows the accuracy and predictions of the new analytic methods to be compared with established results.

In a previous article,[6] to be referred to as paper I, an algorithm was demonstrated for computing values for essentially all quasinormal frequencies for both Schwarzschild and Kerr black holes, and an analytic representation for the quasinormal wave functions was given. The wave functions for arbitrary frequencies are generalized spheroidal wave functions, and a detailed study of these will be found in paper II (Ref. 7). This previous work provides the foundation for the present study, which shows for the first time how a quasinormal mode expansion can be obtained in a convergent form, and solves the problem of divergent source-term integrals. The new analytic representations for the generalized spheroidal wave functions yield a complete description of the branch cut in the frequency parameter of the frequency-domain Green's function, which in turn allows the degree of completeness of the quasinormal modes to be estimated as a function of time subsequent to the arrival of the first response to the perturbation. Many of the known properties of gravitational perturbations to the Schwarzschild geometry can then be expressed in a fashion that reflects the underlying analytic properties of the propagating Green's function. In particular, I will show how each individual quasinormal mode contributes to the overall time response from a perturbation to the black hole, and will demonstrate how the response at times subsequent to the decay of the quasinormal ringing will be characterized by a never-before-postulated *radiating* decay tail.

The analysis described in this article is generalizable to the Newman-Penrose formalism and Teukolsky's equations for perturbations to the Kerr geometry, and the techniques outlined in this paper should prove useful in addressing the question of the excitation of the Kerr

quasinormal modes, including the unstable modes recently suggested by Detweiler and Ove:[8] these applications will be the subject of a future study. The algorithms presented herein are rapid, accurate, and require no numerical integration of the differential equations. They essentially solve the forward problem of the spectral decomposition of gravitational radiation due to perturbations to the Schwarzschild geometry, and should provide a usable computational foundation for the eventual inversion and interpretation of radiation signals from astrophysical black holes.

Outline of the problem

The radial part of the separated partial differential equations that describe small perturbations to the Schwarzschild geometry can be expressed as an inhomogeneous one-dimensional wave equation with a potential:

$$\frac{\partial^2}{\partial r_*^{\,2}}\Psi(r_*,t)-\frac{\partial^2}{\partial t^2}\Psi(r_*,t) - \frac{r-1}{r^3}\left[l(l+1)-\frac{m^2-1}{r}\right]\Psi(r_*,t)=-Q(r_*,t)\,, \tag{1}$$

where $r_*=r+\ln(r-1)$ and the Schwarzschild r and t coordinates have been normalized such that $c=G=2M=1$. Note that the asterisk used to denote the tortoise coordinate can appear interchangeably as both a superscript and as a subscript: r^* is the same as r_*. When a function $f(r_*)$ is written in terms of the Schwarzschild coordinate r, the inverse function, $r(r_*)$, is to be assumed.

The parameter m in (1) denotes the spin of the perturbing field, and takes the values 0, 1, or 2 for components of scalar, electromagnetic, and gravitational fields. When $m=0$ the function $\Psi(r_*,t)$ represents a small scalar perturbation field, and the derivation of Eq. (1) in this case is a straightforward exercise in perturbation theory.[9] Wheeler[10] showed how the components of the electromagnetic field could be expressed in terms of solutions to this equation when $m=1$, while Regge and Wheeler[11] showed how odd-parity (axial) gravitational perturbations to the geometry could be expressed in terms of its solutions when $m=2$. A similar equation obeyed by the components of even-parity (polar) gravitational perturbations, but with a slightly different potential, was derived by Zerilli.[12] Chandrasekhar,[13] and Chandrasekhar and Detweiler,[14] subsequently showed that solutions to Zerilli's even-parity equation could be expressed in terms of the Regge-Wheeler odd-parity solutions. The Teukolsky equations that describe all perturbations to the Kerr geometry via the Newman-Penrose formalism are also generalized spheroidal wave equations, and can be solved by essentially the same methods as those presented here. Equation (1), with appropriate source terms $Q(r_*,t)$, can therefore be considered to be the fundamental differential equation describing perturbations to the Schwarzschild geometry, and the method of its solution will be applicable to nearly all perturbation problems involving uncharged black holes.

The specific relationship between the response function $\Psi(r_*,t)$ and the actual metric perturbations, and between the source function $Q(r_*,t)$ and the stress-energy tensor, are given in the references cited and will not be dealt with in this study. The present concern is a mathematical description of how a general source perturbation $Q(r_*,t)$ is radiated to $r_*=\pm\infty$. The paper is outlined as follows.

Section II demonstrates how the Green's function $G(r_*,t\,|\,r'_*,t')$, that solves Eq. (1) when $Q(r_*,t)=\delta(r-r')\delta(t-t')$, can be expressed as a sum over quasinormal modes, an integral around a branch cut in the complex frequency plane, and a high-frequency remnant of the corresponding free-space propagator. The quasinormal mode sum is expressed in concise analytic form, and the branch cut integral is exactly solvable when $t\gg r_*$, independent of the observer's position r_*.

Section III examines the initial-value problem $Q(r_*,t)=\psi_0(r_*)\delta'(t)+v_0(r_*)\delta(t)$, and analyzes the response both from compact and from analytic sources. Response from the compact sources is given by a simple numeric integration, while an analytic expression for the response from extended sources of the general form

$$\psi_0(r_*)=\sum_{j=1}^{\infty} c_j r^{-k_{1j}}(r-1)^{-k_{2j}}e^{\sigma_{1j}r}\,,$$

$$v_0(r_*)=\sum_{j=1}^{\infty} d_j r^{-k_{3j}}(r-1)^{-k_{4j}}e^{\sigma_{3j}r}\,,$$

is obtained as a series of confluent hypergeometric functions. Sources with $\delta(t)$ and $\delta'(t)$ time dependences may be interpreted in terms of the initial-value problem, the response from which may also be obtained by direct numerical integration of the homogeneous form of Eq. (1) by the method of characteristics. This provides a valuable check on the new results. A unified derivation is given for the amplitudes of the radiative $(t-r_*)^{-l-1}$ and final t^{-2l-2} decay tails.

Section IV addresses the problem of determining the quasinormal mode response for the characteristic-value problem, and results are compared with those of previous studies of gravitational radiation emitted by collapsing relativistic stars.[15–19] In the present study the contributions from the higher-order quasinormal modes are explicitly identified for the first time, and are seen to be significant for $(t-r_*)$ less than approximately 30.

Section V discusses the quasinormal mode response from sources with more general time dependences. The quasinormal model component of the Green's function for the Zerilli equation is derived, and applied to the classic problem of a test particle falling radially into the black hole. The present results are again compared with those of previous workers.[1,2,20]

II. CONSTRUCTION OF THE TIME-DOMAIN GREEN'S FUNCTION

A unique solution to Eq. (1) requires, in addition to the source term $Q(r_*,t)$, the specification of Cauchy data at some initial time $t=t_0$. For general source terms the usual choice requires $\Psi(r_*,t)$ and $\Psi_{,t}(r_*,t)$ to be zero for all times prior to the appearance of the first nonzero $Q(r_*,t)$. Astrophysical sources are frequently of infinite extent in both space and time, with $Q(r_*,t)\to 0$ only as $t\to-\infty$, and in these cases causality requires that $\Psi(r_*,t)\to 0$ as $t\to-\infty$. The time domain Green's function $G(r_*,t\mid r'_*,t')$ is defined to satisfy the differential equation

$$\frac{\partial^2}{\partial r_*^2}G(r_*,t\mid r'_*,t')-\frac{\partial^2}{\partial t^2}G(r_*,t\mid r'_*,t') - V(r_*)G(r_*,t\mid r'_*,t')=-\delta(r_*-r'_*)\delta(t-t')\,, \tag{2}$$

where

$$V(r_*)=\frac{r-1}{r^3}\left[l(l+1)-\frac{m^2-1}{r}\right], \tag{3}$$

subject to the condition that $G(r_*,t\mid r'_*,t')=0$ for $t<t'$. The solution $\Psi(r_*,t)$ to Eq. (1) is then given by[21]

$$\begin{aligned}\Psi(r_*,t)=&\int_{t_0}^{\infty}\int_{-\infty}^{\infty}G(r_*,t\mid r'_*,t')Q(r'_*,t')dr'_*dt'\\&+\int_{-\infty}^{\infty}[G(r_*,t\mid r'_*,t')\Psi_{,t'}(r'_*,t')-\Psi(r'_*,t')G_{,t'}(r_*,t\mid r'_*,t')]_{t'=t_0}dr'_*\\&+\int_{t_0}^{\infty}[G(r_*,t\mid r'_*,t')\Psi_{,r'_*}(r'_*,t')-\Psi(r'_*,t')G_{,r'_*}(r_*,t\mid r'_*,t')]_{r'_*=-\infty}^{r'_*=+\infty}dt'\,,\end{aligned} \tag{4}$$

where t_0 may be either finite or $-\infty$. The last integral is over surface terms at the horizon and spatial infinity: the present radiation boundary conditions require that its contribution vanish.[5] The response function $\Psi(r_*,t)$ is then uniquely determined by the source $Q(r_*,t)$, the initial data $\Psi(r_*,t_0)$, and by the Green's function, which satisfies the important reciprocity relation

$$G(r_*,t\mid r'_*,t')=G(r'_*,-t'\mid r_*,-t)\,. \tag{5}$$

In this section I show how $G(r_*,t\mid r'_*,t')$ can be decomposed into a sum over quasinormal modes, an integral around the branch cut in the frequency parameter, and an integral over asymptotically large magnitudes of the frequency.

A. The frequency-domain Green's function

The frequency-domain Green's function $g(r_*,r'_*,s)$ is obtained by a Laplace transform

$$g(r_*,r'_*,s)=\int_{t'}^{\infty}e^{s(t'-t)}G(r_*,t\mid,r'_*,t')dt\,, \tag{6}$$

and the time-domain function is recovered by the inverse

$$G(r_*,t\mid r'_*,t')=\frac{1}{2\pi i}\int_{\epsilon-i\infty}^{\epsilon+i\infty}e^{s(t-t')}g(r_*,r'_*,s)ds\,. \tag{7}$$

It is important when considering the frequency response of the black hole to distinguish between those frequencies comparable in magnitude to the normalized scale of the hole, and those that are appreciably larger. In this paper $2M$, the dimension of the hole, has been incorporated into the scaling of r and t, so that the low frequencies that strongly characterize the interaction dynamics of the hole are of magnitude $|s|\sim 1$, while "high frequencies" are typically of order $|s|>10$. The differential equation satisfied by the frequency-domain Green's function $g(r_*,r'_*,s)$ is

$$\frac{d^2}{dr_*^2}g(r_*,r'_*,s)-\left[s^2+\frac{r-1}{r^3}\left[l(l+1)-\frac{m^2-1}{r}\right]\right]\times g(r_*,r'_*,s)=-\delta(r_*-r'_*)\,. \tag{8}$$

The solution, in a notation similar to that used by Detweiler,[3] can be expressed

$$g(r_*,r'_*,s)=W^{-1}(s)\psi_{r_+}(r_{*<},s)\psi_{\infty_+}(r_{*>},s)\,, \tag{9}$$

where $r_{*<}=\min(r_*,r'_*)$, $r_{*>}=\max(r_*,r'_*)$, and $W(s)$ is the Wronskian of the two independent homogeneous solutions ψ_{∞_+} and ψ_{r_+}. The event horizon is at $r_*=-\infty$, or $r=r_+=1$. A third useful homogeneous solution is denoted by $\psi_{\infty_-}(r_*,s)$. The homogeneous solutions are defined by their asymptotic properties:

$$\begin{aligned}&\lim_{r_*\to-\infty}\psi_{r_+}(r_*,s)\sim e^{sr_*}\,,\\&\lim_{r_*\to+\infty}\psi_{r_+}(r_*,s)\sim A_{\rm in}(s)e^{sr_*}+A_{\rm out}(s)e^{-sr_*}\,,\end{aligned} \tag{10}$$

$$\begin{aligned}&\lim_{r_*\to+\infty}\psi_{\infty_+}(r_*,s)\sim e^{-sr_*}\,,\\&\lim_{r_*\to-\infty}\psi_{\infty_+}(r_*,s)\sim B_{\rm in}(s)e^{sr_*}+B_{\rm out}(s)e^{-sr_*}\,,\end{aligned} \tag{11}$$

$$\begin{aligned}&\lim_{r_*\to+\infty}\psi_{\infty_-}(r_*,s)\sim e^{sr_*}\,,\\&\lim_{r_*\to-\infty}\psi_{\infty_-}(r_*,s)\sim B_{\rm out}(-s)e^{sr_*}+B_{\rm in}(-s)e^{-sr_*}\,.\end{aligned} \tag{12}$$

These solutions are not all three independent, being related by

$$\psi_{r_+}(r_*,s)=A_{\rm in}(s)\psi_{\infty\_}(r_*,s)+A_{\rm out}(s)\psi_{\infty+}(r_*,s) \tag{13}$$

and

$$B_{\rm out}(s)=A_{\rm in}(s),\quad B_{\rm in}(s)=-A_{\rm out}(-s)\ ,$$
$$A_{\rm in}(s)A_{\rm in}(-s)-A_{\rm out}(s)A_{\rm out}(-s)=1\ . \tag{14}$$

The transmission and reflection amplitudes are defined by

$$T(s)\equiv\frac{1}{A_{\rm in}(s)},\quad R(s)\equiv\frac{A_{\rm out}(s)}{A_{\rm in}(s)}\ ,$$

and the Wronskian of $\psi_{\infty+}$ and ψ_{r_+} is

$$W(s)=\psi_{\infty+}\psi_{r_+,r_*}-\psi_{r_+}\psi_{\infty+,r_*}=2sA_{\rm in}(s)\ . \tag{15}$$

The corresponding Wronskian of $\psi_{\infty\_}$ and ψ_{r_+} is equal to $-2sA_{\rm out}$. It is convenient to express $\psi_{r_+}(r_*,s)$ and the $\psi_{\infty\pm}(r_*,s)$ in terms of the Schwarzschild coordinate r, wherein they satisfy the differential equation

$$r(r-1)\psi_{,rr}+\psi_{,r}-\left[\frac{r^3s^2}{r-1}+l(l+1)-\frac{m^2-1}{r}\right]\psi=0\ .$$

Equation (16) is a generalized spheroidal wave equation. Analytic expressions for the solutions ψ_{r_+}, $\psi_{\infty+}$, and $\psi_{\infty\_}$, as discussed in Appendix A and in paper II, are

$$\psi_{r_+}(r,s)=r^{-2s}(r-1)^s e^{-s(r-2)}\sum_{n=0}^{\infty}a_n(1-1/r)^n\ , \tag{17}$$

$$\psi_{\infty\pm}(r,s)=(2is)^{\pm s}e^{\pm i\phi_\pm}(1-1/r)^s\sum_{L=-\infty}^{\infty}b_L[G_{L+\nu}(\eta,\rho)\pm iF_{L+\nu}(\eta,\rho)]\ , \tag{18}$$

where $G_{L+\nu}(\eta,\rho)$ and $F_{L+\nu}(\eta,\rho)$ are Coulomb wave functions with $\eta=-is$ and $\rho=isr$. The expansion coefficients a_n and b_L satisfy three-term recurrence relations, and Eq. (10) requires the a_n be normalized such that $a_0=1$. The phase parameter ν is chosen such that the b_L are minimal as $L\to\pm\infty$. The a_n are minimal as $n\to\infty$ when $s=s_q$, a quasinormal frequency. The normalization phases ϕ_+ and ϕ_- are given by

$$\phi_\pm=\pm i\ln\left[\sum_{L=-\infty}^{\infty}b_L[\Gamma(L+\nu+1+s)/\Gamma(L+\nu+1-s)]^{\pm1/2}e^{\mp i(L+\nu)\pi/2}\right]\ . \tag{19}$$

Expansions (17), (18), and (19) may be accurately evaluated over a wide range of complex values of r and s.

B. The time-domain Green's function

The Schwarzschild quasinormal frequencies occur in complex-conjugate pairs s_q and $\bar{s}_q$. They are the zeros of $A_{\rm in}(s)$, and hence the poles[22] of $g(r_*,r'_*,s)$. Near these frequencies the amplitude $A_{\rm in}(s)$ may be approximated by[23]

$$\lim_{s\to s_q}A_{\rm in}(s)\sim(s-s_q)dA_{\rm in}(s)/ds\equiv(s-s_q)\alpha_q\ . \tag{20}$$

The complex conjugate of this equation holds for the complex-conjugate frequencies $\bar{s}_q$, and derivatives $\bar{\alpha}_q$. By Eqs. (9), (15), and (20), we can approximate the frequency-domain Green's function near the pole s_q by

$$\lim_{s\to s_q}g(r_*,r'_*,s)\sim\lim_{s\to s_q}\frac{\psi_{r_+}(r_{*<},s)\psi_{\infty+}(r_{*>},s)}{2s(s-s_q)\alpha_q}\ . \tag{21}$$

The contour for the inversion integral (7) for $G(r_*,t\mid r'_*,t')$ may be deformed as illustrated in Fig. 1, and the time-domain Green's function expressed as three distinct terms:

$$G(r_*,t\mid r'_*,t')=G_F(r_*,t\mid r'_*,t')+G_Q(r_*,t\mid r'_*,t')+G_B(r_*,t\mid r'_*,t')\ , \tag{22}$$

where G_Q is the sum of the residues at the poles of $g(r_*,r'_*,s)$, G_B is the integral of $g(r_*,r'_*,s)$ around the branch cut in s, and G_F is the integral along the large $|s|$ quarter circles. It is G_F that propagates the high-frequency response, and which reduces to the free-space Green's function in the limit as the mass of the black hole goes to zero. The low-frequency ringing and late-time decay tails, that together give radiation phenomena involving black holes its distinct character, are, respectively, described by G_Q and G_B, and it is these two functions that are the subjects of the present investigation. Figure 1 and Eqs. (7) and (21) give the residue sum as

$$G_Q(r_*,t\mid r'_*,t')=\sum_{q=1}^{\infty}\frac{\psi_{r_+}(r_{*<},s_q)\psi_{\infty+}(r_{*>},s_q)e^{s_q(t-t')}}{2s_q\alpha_q}+\sum_{q=1}^{\infty}\frac{\psi_{r_+}(r_{*<},\bar{s}_q)\psi_{\infty+}(r_{*>},\bar{s}_q)e^{\bar{s}_q(t-t')}}{2\bar{s}_q\bar{\alpha}_q}\ , \tag{23}$$

while

$$G_B(r_*,t\mid r'_*,t')=\frac{1}{2\pi i}\int_0^{-\infty}[g(r_*,r'_*,s+i\epsilon)-g(r_*,r'_*,s-i\epsilon)]e^{s(t-t')}ds\ . \tag{24}$$

Numerical studies by Vishveshwara,[24] Press,[25] Price,[15] Davis, Ruffini, and Tiomno,[2] Cunningham, Price, and Moncrief,[16] Detweiler and Szedenits,[5] Detweiler,[4] and Smarr[26] show that quasinormal ringing will dominate the response at all but very early and very late times; therefore I will discuss the evaluation of G_Q first.

1. Contribution from the quasinormal modes

At the quasinormal frequencies s_q the functions ψ_{r_+} and ψ_{∞_+} are proportional:

$$\psi_{r_+}(r_*,s_q)/\psi_{\infty_+}(r_*,s_q)=A_{\text{out}}(s_q) =e^{2s_q}\sum_{n=0}^{\infty}a_n(s_q)\ . \tag{25}$$

Since $a_n(\bar{s})=\bar{a}_n(s)$ (see Appendix A), it follows at the complex-conjugate quasinormal frequencies $\bar{s}_q$ that $A_{\text{out}}(\bar{s}_q)=\bar{A}_{\text{out}}(s_q)$. As any physical observation of quasinormal ringing will be done at large values of r_*, it is natural to define normalized quasinormal mode wave functions $\psi_q(r_*)$ by

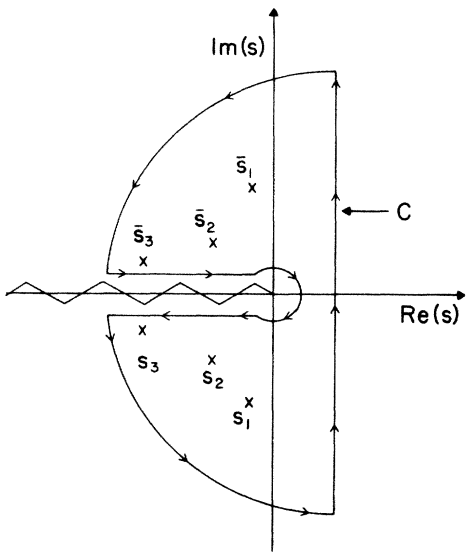

FIG. 1. Inversion contour for

$$G(r_*,t\mid r'_*,t')=(2\pi i)^{-1}\int_{\epsilon-i\infty}^{\epsilon+i\infty}g(r_*,r'_*,s)e^{s(t-t')}ds\ ,$$

Eq. (7). A few of the infinity of quasinormal frequencies and their complex conjugates are indicated by $\times$. These are the s poles of $g(r_*,r'_*,s)$. The desired integral extends along the vertical line from $s=-i\infty$ to $s=+i\infty$, and is obtained for $t>t'$ by closing the contour as shown and subtracting the integral around the branch cut. The contribution from the two quarter circles at $|s|=\infty$ is not considered in the present study. Note the convention used in this paper: the s_q are defined to lie in the third quadrant of the complex s plane, while their complex conjugates, $\bar{s}_q$, lie in the second.

$$\psi_q(r_*)=A_{\text{out}}{}^{-1}(s_q)e^{s_q r_*}\psi_{r_+}(r_*,s_q) =\left[\frac{r-1}{r}\right]^{2s_q}\frac{\sum_{n=0}^{\infty}a_n(s_q)(1-1/r)^n}{\sum_{n=0}^{\infty}a_n(s_q)}\ . \tag{26}$$

The $\psi_q(r_*)$ diverge like $e^{2s_q(r_*-1)}$ as $r\to 1$, and go to unity as $r_*\to\infty$. The quasinormal mode contribution to Eq. (22) can then be written

$$G_Q(r_*,t\mid r'_*,t') =2\,\text{Re}\left[\sum_{q=1}^{\infty}\frac{\psi_q(r_*)\psi_q(r'_*)e^{s_q(t-t'-r_*-r'_*)}}{2s_q\alpha_q A_{\text{out}}{}^{-1}(s_q)}\right]\ . \tag{27}$$

The coefficient $A_{\text{out}}(s_q)$ and the derivative α_q are both proportional to the first expansion coefficient a_0; hence expression (27) is independent of the normalization of ψ_{r_+}. The computation of the α_q is discussed in Appendix A.

2. Convergence of the quasinormal mode sum

Although I cannot yet give a complete answer to the question of the convergence of series (27), an argument approximately valid for large values of r_* and r'_* suggests itself from the values of $A_{\text{out}}(s_q)/(2s_q\alpha_q)$ listed in Table I.

For large r_* and r'_* the quasinormal sum G_Q becomes

$$G_Q(r_*,t\mid r'_*,t')\sim 2\,\text{Re}\left[\sum_{q=1}^{\infty}\frac{e^{s_q(t-t'-r_*-r'_*)}}{2s_q\alpha_q A_{\text{out}}{}^{-1}(s_q)}\right]\ , \tag{28}$$

and the ratio of successive terms in this series is

$$\left[\frac{s_q\alpha_q A_{\text{out}}(s_{q+1})}{s_{q+1}\alpha_{q+1}A_{\text{out}}(s_q)}\right]e^{(s_{q+1}-s_q)(t-t'-r_*-r'_*)}\ . \tag{29}$$

If, for the sake of argument, one assumes that the magnitude of the term in large parentheses goes to unity for large q, then the magnitude of successive terms in series (28), from values of s_q listed in Table I, goes asymptotically as $\exp[-(t-t'-r_*-r'_*)/2]$, in which case the quasinormal mode expansion $G_Q(r_*,t\mid r'_*,t')$ converges for large r_* and r'_* if $(t-t'-r_*-r'_*)>0$. This is the type of convergence behavior one would expect from a quasinormal mode expansion, as can be seen if one considers as an initial source an impulse located at $r'\gg 1$ at time t', that is moving inward toward the horizon with velocity $\beta=1$. This impulse will pass an observer located at a position r slightly less than r' long before it interacts with the highly curved geometry of the black hole, and the quasinormal modes cannot be expected to represent the impulse as it passes the observer going inward. This is the role of the free-space propagator G_F. Part of this ingoing initial perturbation is eventually reflected from the curvature potential near the event horizon back to spatial infinity, and it is this reflective interaction that excites the quasinormal ringing. The initial response from the reflected component will pass the observer at a time

TABLE I. Selected values of the quasinormal frequencies s_q, transmission amplitude derivatives $\alpha_q \equiv dA_{\text{in}}(s)/ds \mid_{s=s_q}$, and normalization factors $A_{\text{out}}(s_q)$. The parameter l is the multipole moment, and m denotes the field's spin.

l	m	s_q	α_q	$\frac{A_{\text{out}}}{2s_q\alpha_q}$
1	1	(−0.184 98,−0.496 53)	(−5.903 73,−1.817 80)	(−0.161 40,0.011 86)
1	1	(−0.587 34,−0.429 03)	(−3.656 81,2.839 26)	(0.011 77,0.180 94)
1	1	(−1.050 38,−0.349 55)	(−2.244 9,5.134 1)	(0.081 57,−0.072 11)
1	1	(−1.543 82,−0.292 35)	(−1.505,6.741)	(−0.061 97,0.018 72)
2	2	(−0.177 92,−0.747 34)	(0.098 66,−5.219 40)	(0.126 90,0.020 32)
2	2	(−0.547 83,−0.693 42)	(−2.449 04,−1.160 95)	(0.047 68,−0.223 76)
2	2	(−0.956 55,−0.602 11)	(−2.428 32,1.028 26)	(−0.190 28,0.015 75)
2	2	(−1.410 30,−0.503 01)	(−2.001 05,2.582 29)	(0.080 87,0.079 61)
2	2	(−1.893 69,−0.415 03)	(−1.583 71,3.823 22)	(−0.017 10,−0.060 53)
2	2	(−2.391 22,−0.338 60)	(−1.186 76,4.765 34)	(−0.001 69,0.036 43)
2	2	(−2.895 82,−0.266 50)	(−0.132 08,4.069 06)	(0.010 67,−0.027 41)
3	2	(−0.185 41,−1.198 89)	(4.070 78,1.060 36)	(−0.093 90,−0.049 19)
3	2	(−0.562 60,−1.165 29)	(0.830 36,−1.345 51)	(−0.151 13,0.269 77)
3	2	(−0.958 19,−1.103 37)	(−0.555 62,−1.003 80)	(0.415 04,0.141 01)
3	2	(−1.380 67,−1.023 92)	(1.139 03,0.282 53)	(0.043 38,0.412 72)
4	2	(−0.188 33,−1.618 36)	(1.563 66,−3.285 71)	(−0.065 35,−0.065 24)
4	2	(−0.568 67,−1.593 26)	(−0.834 11,−0.667 66)	(−0.261 47,0.251 52)
4	2	(−0.959 82,−1.545 42)	(−0.539 05,0.293 36)	(0.549 26,0.435 31)
4	2	(−1.367 85,−1.479 67)	(−0.039 82,0.510 68)	(0.316 88,−0.837 88)

$t \simeq t' + r + r'$, and it is from this time onward that the quasinormal modes can be expected to contribute to the observed response. This behavior is illustrated in Fig. 2 for an electric dipole field, where the initial impulse source is approximated by a unit Gaussian centered at $r'=28$ at $t'=0$, and the observer is positioned at $r=25$. The first four modes adequately represent the response for $t-t-r' > 10$, and the addition of more modes will probably improve the representation for earlier times. Thus far, however, the most α_q I have been able to calculate is the first seven for the $l=2$ gravitational modes. The ninth $l=2$ gravitational quasinormal frequency is computed to lie very near the negative real s axis within round-off error of $s=-4$, and probably does not contribute strongly to the sum. The ultimate convergence of series (27) depends on the presently unknown values of $A_{\text{out}}(s_q)/(2s_q\alpha_q)$ for the tenth and higher modes. Therefore, while the present results strongly suggest convergence, they are unable to give a precise lower limit for the time t at which the convergence starts, and indeed do not exclude the possibility that at series (27) may be asymptotic. Further, the completeness of the quasinormal mode sum must decrease at early times, as it depends on the relative contribution from the branch cut integral G_B. I will discuss this integral next, and show that its magnitude, while decreasing rapidly for $(t-t'-r_*-r'_*) > 1$, may become quite large (and perhaps infinite) as $(t-t'-r_*-r'_*) \to 0$.

3. *Late-time response and the integral around the branch cut*

The branch cut integral G_B is interesting. It contributes heavily to the initial burst of radiation near $(t-t'-r_*-r'_*)=0$, decreases rapidly for $(t-t'-r_*-r'_*) > 1$, but also gives rise to the late time power-law decay tail that eventually dominates the exponentially decaying quasinormal ringing. The branch cut in $g(r_*,r'_*,s)$ is itself due to the branch cut in $\psi_{\infty_+}(r_*,s)$, and the branch cut integral can be written

$$G_B(r_*,t \mid r'_*,t') = \frac{1}{2\pi i} \int_0^{-\infty} \psi_{r_+}(r_{*<},s) \left[\frac{\psi_{\infty_+}(r_{*>},s\,e^{2\pi i})}{W(s\,e^{2\pi i})} - \frac{\psi_{\infty_+}(r_{*>},s)}{W(s)} \right] e^{s(t-t')} ds \ , \tag{30}$$

where s is taken to lie on the bottom of the branch cut, and $s\,e^{2\pi i}$ on the top. The value of ψ_{∞_+} on each side of the branch cut may be determined from the analysis of generalized spheroidal wave functions given in paper II, and Eq. (128) of that paper can be applied to the present equation (18) to give

$$\psi_{\infty_+}(r_*,s\,e^{2\pi i}) = \psi_{\infty_+}(r_*,s) - K(s)\psi_{\infty_-}(r_*,s) \ , \tag{31}$$

where the function $K(s)$ is defined by

$$K(s)\equiv(1-e^{2\pi i(s-\nu)})(2is)^{2s}e^{i(\phi_+ +\phi_-)}, \tag{32}$$

and

$$e^{i(\phi_+ +\phi_-)}=\frac{\sum_{L=-\infty}^{\infty} b_L[\Gamma(L+\nu+1-s)/\Gamma(L+\nu+1+s)]^{-1/2}e^{+i(L+\nu)\pi/2}}{\sum_{L=-\infty}^{\infty} b_L[\Gamma(L+\nu+1-s)/\Gamma(L+\nu+1+s)]^{+1/2}e^{-i(L+\nu)\pi/2}} . \tag{33}$$

Equations (10) and (31) then enable us to evaluate the Wronskian (15) on the top of the cut:

$$W(s\,e^{2\pi i})=2sA_{\rm in}(s)+2sK(s)A_{\rm out}(s) . \tag{34}$$

Equations (31) and (34) allow expression (30) for G_B to be reduced to an integral on just the lower side of the branch cut:

$$G_B(r_*,t\mid r'_*,t')=-\frac{1}{2\pi i}\int_0^{-\infty}\frac{e^{s(t-t')}\psi_{r_+}(r_{*<},s)K(s)[A_{\rm in}\psi_{\infty\_}+A_{\rm out}\psi_{\infty\_+}(r_{*>},s)]}{2sA_{\rm in}(s)[A_{\rm in}(s)+K(s)A_{\rm out}(s)]}ds . \tag{35}$$

Relation (13) then gives the final result

$$G_B(r_*,t\mid r'_*,t')=-\frac{1}{2\pi i}\int_0^{-\infty}\frac{e^{s(t-t')}K(s)\psi_{r_+}(r_{*<},s)\psi_{r_+}(r_{*>},s)}{2sA_{\rm in}(s)[A_{\rm in}(s)+K(s)A_{\rm out}(s)]}ds . \tag{36}$$

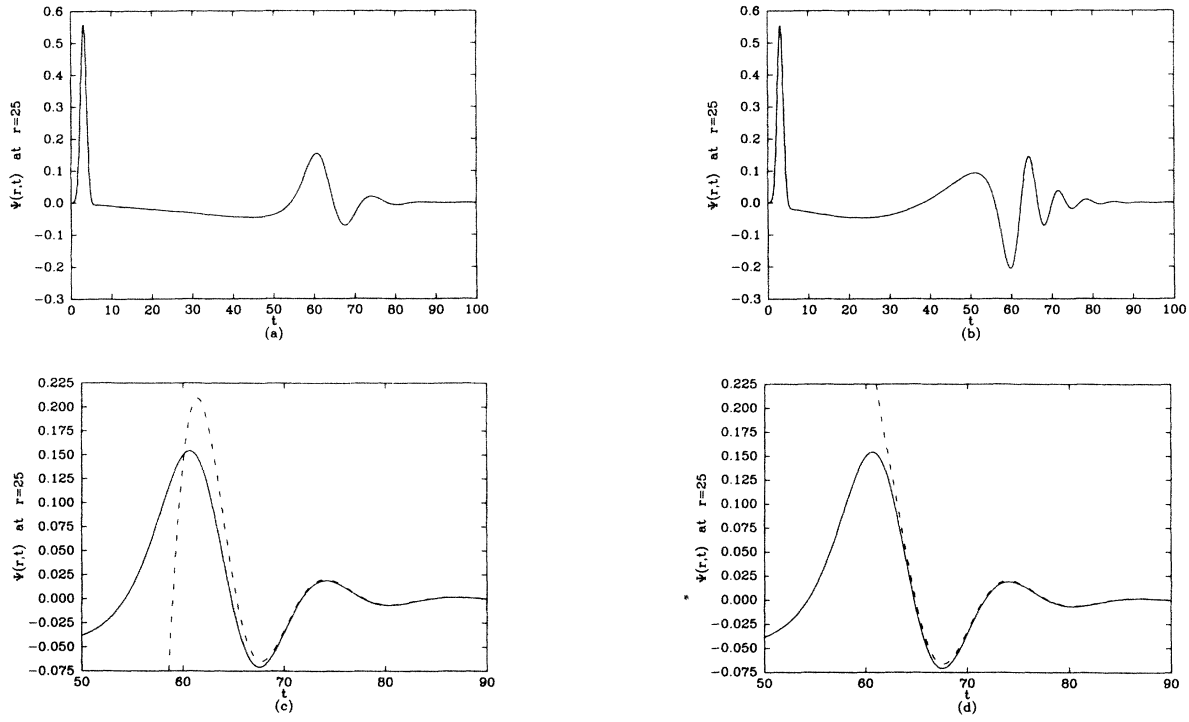

FIG. 2. Time response of Eq. (1) due to a source

$$q(r'_*,t)=\pi^{-1/2}[e^{-(r'-r_0)^2}\delta'(t)-2(r'-r_0)e^{-(r'-r_0)^2}\delta(t)] ,$$

corresponding to a unit Gaussian distribution initially centered at r_0, and moving toward the horizon with velocity factor $\beta=1$. Here $r_0=28$, and the point of observation is $r_{\rm obs}=25$. The solid curves represent the complete solution to Eq. (1) as determined by direct numerical integration by the method of characteristics. (a) is for an electric dipole field, for which $l=1$ and $m=1$ in Eq. (1). The spike at $t=3=r_0^*-r_{\rm obs}^*$ is just the initial Gaussian as it moves inward past the observer. The next prominent maximum, at $t=60\approx r_0^*+r_{\rm obs}^*$, is the component of the initial Gaussian that is reflected (with dispersion) back from the Regge-Wheeler potential outside $r=1$. The quasinormal modes cannot contribute to the response before this time, but are responsible for all the subsequent oscillations. (b) is a similar curve for an electric quadrupole source, $l=2$ and $m=1$. The inverted peak at $t=60$ is a consequence of Eq. (42), the reflected amplitude being given by $R\equiv A_{\rm out}(s)/A_{\rm in}(s)$. Note the increased dispersion over that for $l=1$: a detailed analysis of the G_F and G_B will be necessary before the nature of this precursor dispersion can be understood. (c) and (d) are details of the ringing region of (a). The dashed curve in (c) represents the contribution from the fundamental quasinormal mode, $q=1$ in Eq. (49), while in (d) the dashed curve represents the response from the first two modes, $q=1,2$.

The quantity $\nu \pm s$ is an integer only as $s \to 0$ and, for gravitational fields, at the algebraically special frequency $s_a = -\frac{1}{6} l(l-1)(l+1)(l+2)$. At these points $K(s)$ is still well behaved, since the poles in the γ functions are canceled by the zero of $\{1-\exp[2\pi i(s-\nu)]\}$. By definition, $A_{\text{in}}(s)$ and $A_{\text{out}}(s)$ cannot have any simultaneous zeros, so there are no infinities in the integrand of expression (36) if $(t-t'-r_*-r'_*)$ is greater than approximately zero. Expression (36) can now be integrated, in principle, for any r_*, r'_*, t, and t'. An estimate of the magnitude of G_B can be made by considering the limit where r and r' are both much larger than unity. In this limit, by Eqs. (10)–(12),

$$G_B(r_*,t \mid r'_*,t') = -\frac{1}{2\pi i}\int_0^{-\infty} \frac{K(s)A_{\text{in}}(s)}{2s[A_{\text{in}}(s)+K(s)A_{\text{out}}(s)]} e^{s(t-t'+r_*+r'_*)} ds$$
$$-\frac{1}{2\pi i}\int_0^{-\infty} \frac{K(s)A_{\text{out}}(s)}{s[A_{\text{in}}(s)+K(s)A_{\text{out}}(s)]} \cosh[s(r_*-r'_*)] e^{s(t-t')} ds$$
$$-\frac{1}{2\pi i}\int_0^{-\infty} \frac{K(s)A_{\text{out}}{}^2(s)}{2sA_{\text{in}}(s)[A_{\text{in}}(s)+K(s)A_{\text{out}}(s)]} e^{s(t-t'-r_*-r'_*)} ds \ . \tag{37}$$

Equation (37) may be further simplified through the introduction of the transmission and reflection amplitudes $T(s) \equiv A_{\text{in}}{}^{-1}(s)$ and $R(s) \equiv A_{\text{out}}(s)/A_{\text{in}}(s)$. The amplitudes $A_{\text{in}}(s)$ and $A_{\text{out}}(s)$ both become infinite, such that $T(s) \to 0$ while $R(s)$ remains finite, at values of the frequency parameter $s = -n/2$ for $n = 0,1,2,\ldots$, although it is difficult to speak of the black hole as completely reflecting "waves" with these frequencies because, with the important exception of $s=0$ [where $|R(s)|=1$], the actual frequency values $\omega = is$ are purely imaginary. Since the infinities of A_{in} and A_{out} are of the same relative size, the integrands in Eq. (37) remain finite and the integrals all converge, at least if $(t-t'-r_*-r'_*)>0$. As $s \to 0$ the function $K(s) \to -2\pi i s\, e^{l\pi i}$, while $\psi_{r_+}(r_*,s)$ remains finite for finite r. The integrand of Eq. (36) then vanishes as $s \to 0$, and the magnitude of G_B usually decreases faster than $(t-t'-r_*-r'_*)^{-1}$ as $(t-t'-r_*-r'_*)$ becomes much larger than about one. The quasinormal modes at intermediate times then become essentially complete, until at late times they decay beneath the power-law tail.

4. *Late-time decay tails*

Considerable simplification of expression (36) for G_B is obtained in the important case $(t-t'-r_*-r'_*) \gg 1$, for then only $|s| \ll 1$ will contribute to the integral. From results given in Sec. VI C of paper II, the $s \to 0$ limiting forms for ν, ψ_{r_+}, ψ_{∞_+}, and ψ_{∞_-} can be found to be

$$\lim_{s\to 0} \nu \sim l + O(s^2) \ , \tag{38}$$

$$\lim_{s\to 0} \psi_{r_+}(r,s) \sim (2\nu+1)!!(is)^{-\nu-1}(1-r^{-1})^s F_\nu(-is,isr) \ , \tag{39}$$

$$\lim_{s\to 0} \psi_{\infty_\pm}(r,s) \sim (1-r^{-1})^s [G_\nu(-is,isr) \pm iF_\nu(-is,isr)] e^{\pm i\nu\pi/2} \ . \tag{40}$$

Other necessary relations are

$$\lim_{s\to 0} K(s) \sim -2\pi i s\, e^{\nu\pi i} \ , \tag{41}$$

$$\lim_{s\to 0} A_{\text{out}}(s) \sim -e^{i\nu\pi} \lim_{s\to 0} A_{\text{in}}(s) \ , \tag{42}$$

$$\lim_{s\to 0} 2sA_{\text{in}}(s) \sim (2\nu+1)!!(s)^{-\nu} \ . \tag{43}$$

The last result follows from Eqs. (39) and (40) and the Wronskian relation for the Coulomb wave functions, $F_{l,\rho}(\eta,\rho)G_l(\eta,\rho) - G_{l,\rho}(\eta,\rho)F_l(\eta,\rho) = 1$. The limiting relationship between $A_{\text{in}}(s)$ and $A_{\text{out}}(s)$ is a result of (39) and the fact that $F_l(-is,isr) \sim \sin(isr_* - l\pi/2)$ in the limit as $s \to 0$ and $|isr| \to \infty$, and is an expression of the property that the black hole completely reflects very low-frequency radiation.[24]

This last set of expressions yields, from Eq. (36), the final result for the limit that $(t-t'-r_*-r'_*) \gg 1$:

$$G_B(r_*,t \mid r'_*,t') \sim -2\int_0^{-\infty} (1-1/r)^s (1-1/r')^s F_l(-is,isr)F_l(-is,isr') e^{s(t-t')} ds \ . \tag{44}$$

If r and r' are not too near unity, $(1-1/r)^s \approx 1$ and this integral may be taken to be that given by Gradshteyn and Ryzhik[27] [Eq. (6.626)], if one uses the approximation

$$\lim_{s\to 0} F_l(-is,isr) \sim isrj_l(isr) \ ,$$

where j_l is the regular spherical Bessel function. If $|sr| \gg 1$, with $|s|$ remaining small, then $j_l(isr)$ must be replaced by $j_l(isr_*)$. Integral (44) simplifies to a single term for two important contributions of r_* and r'_*.

(1) $r_* - r'_* \ll t - t'$ and $(t-t'-r_*+r'_*)/r_* \ll 1$. These are the astrophysically significant radiation zone

conditions for which

$$F_l(-is,isr')\sim[(2l+1)!!]^{-1}(isr')^{l+1},$$

but

$$F_l(-is,isr)\sim\sin(isr_*-l\pi/2).$$

In this case

$$G_B(r_*,t\mid r'_*,t')\sim(-1)^{l+1}\frac{(l+1)!}{(2l+1)!!}(r')^{l+1}(t-t'-r_*)^{-l-2}. \quad (45)$$

(2) $r'_* \ll t-t'$ and $r_* \ll t-t'$. This case gives rise to the very-late-time nonradiating tails first discovered by Price,[15] who considered extended source fields (Secs. III and IV). In this limit

$$F_l(is,-isr')\sim[(2l+1)!!]^{-1}(-isr')^{l+1},$$

and

$$F_l(is,-isr)\sim[(2l+1)!!]^{-1}(-isr)^{l+1},$$

which gives

$$G_B(r_*,t\mid r'_*,t')\sim(-)^{l+1}\frac{2(2l+2)!}{[(2l+1)!!]^2}(rr')^{l+1}(t-t')^{-2l-3}. \quad (46)$$

Equations (22), (27), (46), and (45) form a useful computational definition for the low-frequency part of the time-domain Green's function that propagates small perturbations to the Schwarzschild geometry. This analysis of the Green's function shows that the response functions for perturbations originating far from the horizon and as seen by a distant observer, as typified by Fig. 2, can be broken into approximately six distinct time regions.[29]

(i) $t\approx t'+|r_*-r'_*|$. If the perturbation possesses an initial component moving in the direction of the observer, that component will pass the observer at about this time. It is propagated by the free-space, or high-frequency, remnant that I denote by G_F.

(ii) $t'+|r_*-r'_*|<t<t'+r_*+r'_*$. Precursor region. The nonzero value of the response in this region are due to the dispersiveness of G_F, and possibly a contribution from G_B. Much additional work will be necessary to understand the relative interactions of the two contributing parts of the propagator.

(iii) $t\approx t'+r_*+r'_*$. Initial burst and onset of ringing. The contribution of both G_B and G_Q is greatest at this time, and there is probably much cancellation of their effects, as both the quasinormal mode sum (27) and the branch cut integral (36) appear not to be uniformly convergent as t approaches approximately this value from above. As in the previous case, more study will be needed to clarify the relative contributions of G_B and G_Q near this time.

(iv) $t'+r_*+r'_*<t<t'+r_*+r'_*+\ln[(r')^{l+1}(t-t'-r_*)^{-l-2}]/\mathrm{Re}(s_1)$. Ringing region. From Eq. (45), this is the region in which the response is dominated by the quasinormal ringing, before the exponential decay of G_Q subsides beneath the power-law decay of G_B.

(v) $t'+r_*+r'_*+\ln[(r')^{l+1}(t-t'-r_*)^{-l-2}]/\mathrm{Re}(s_1)<t, r_*-r'_*\ll t-t'$, and $(t-t'-r_*+r'_*)/r_*\ll 1$. Late time radiating decay tail, as specified by Eq. (45).

(vi) $t/r_*\gg 1$. Very-late time nonradiating decay, as specified by Eq. (46).

Even though the power-law decay tail is now shown to radiate, it is extremely weak, and will be very difficult to detect.

III. THE INITIAL-VALUE PROBLEM AND THE RESPONSE FROM A SPATIALLY EXTENDED SOURCE

Equations (4) and (22) can be combined to give

$$\begin{aligned}\Psi(r_*,t)&=\int\int G_F(r_*,t\mid r'_*,t')Q(r'_*,t')dr'_*dt'+\int\int G_Q(r_*,t\mid r'_*,t')Q(r'_*,t')dr'_*dt'\\&\quad+\int\int G_B(r_*,t\mid r'_*,t')Q(r'_*,t')dr'_*dt'\\&\equiv\Psi_F(r_*,t)+\Psi_Q(r_*,t)+\Psi_B(r_*,t),\end{aligned} \quad (47)$$

where $\Psi_F(r_*,t)$ is the response from the high-frequency propagator, $\Psi_Q(r_*,t)$ is the response from the quasinormal modes, and $\Psi_B(r_*,t)$ is the contribution from the integral around the branch cut. We have already seen that the quasinormal modes form the dominant part of the response after the initial burst, and Eq. (27) allows the quasinormal mode response from $Q(r_*,t)$ to be written, assuming Q is real for real r and t, as

$$\begin{aligned}\Psi_Q(r_*,t)&=\int_{-\infty}^{+\infty}\int_{-\infty}^{+\infty}G_Q(r_*,t\mid r'_*,t')Q(r'_*,t')dr'_*dt'\\&=2\,\mathrm{Re}\left[\sum_{q=1}^{\infty}\frac{\psi_q(r_*)e^{s_q(t-r_*)}}{2s_q\alpha_q A_{\mathrm{out}}{}^{-1}(s_q)}\int_{-\infty}^{+\infty}\int_{-\infty}^{+\infty}e^{-s_q(t'+r'_*)}\psi_q(r'_*,t')Q(r'_*,t')dr'_*dt'\right].\end{aligned} \quad (48)$$

It is convenient to express (48) as

$$\Psi_Q(r_*,t)=2\,\mathrm{Re}\left[\sum_{q=1}^{\infty}C_q\psi_q(r_*)e^{s_q(t-r_*)}\right], \quad (49)$$

where the excitation coefficients C_q are defined by

$$C_q\equiv\frac{A_{\mathrm{out}}(s_q)}{2s_q\alpha_q}\int_{-\infty}^{+\infty}\int_{-\infty}^{+\infty}e^{-s_q(t'+r'_*)}\psi_q(r'_*)Q(r'_*,t')\times dr'_*dt'. \quad (50)$$

Since $\mathrm{Re}(s_q)<0$, the excitation coefficient integral (50) shows a marked propensity toward divergence if $Q(r_*,t)$ is of noncompact support (infinite extent) in either r_* or t. This is always the case for physically realizable source terms, which must be analytic at least in r_*. The classical normal modes of closed mechanical systems are Stürm-Liouville eigenfunctions of the wave equation, and their excitation coefficients are just the weighted integral of the driving term over the mode. The classical eigenfunctions are always bounded, and the integrals always converge. The divergence of the corresponding quasinormal mode integral, Eq. (60), is the striking difference between quasinormal ringing and classical resonance,[14] and the divergence of this source-term integral has been the major impediment to the proposed interpretation of quasinormal mode decompositions of the radiation response from perturbations to black holes.

However, the fact that the function $Q(r_*,t)$ is analytic, while necessarily resulting in formal divergence of the integral, is also the key to its successful evaluation. To illustrate this I consider in detail the case of the initial-value problem for the homogeneous wave equation:

$$\frac{\partial^2}{\partial r_*^{\,2}}\Psi(r_*,t)-\frac{\partial^2}{\partial t^2}\Psi(r_*,t) -\frac{r-1}{r^3}\left[l(l+1)-\frac{m^2-1}{r}\right]\Psi(r_*,t)=0\ , \tag{51}$$

where $\Psi(r_*,t_0)=\psi_0(r_*)$ and $\Psi_{,t}(r_*,t_0)=v_0(r_*)$. This may be treated as a special case of the inhomogeneous equation by setting $Q(r_*,t)=\psi_0(r_*)\delta'(t-t_0)+v_0(r_*)\delta(t-t_0)$ in Eq. (1) (Ref. 28). The distribution δ' is defined by the derivative property $\int_{-\epsilon}^{+\epsilon} f(t)\delta'(t)dt=-f'(0)$. While the δ-function time dependences are hardly analytic, the treatment of the spatial part of the integral gives a flavor of how the integration of sources with more general time dependences can be handled (Secs. IV and V, below).

The excitation coefficients for the initial-value problem are then

$$C_q=\frac{A_{\mathrm{out}}(s_q)}{2s_q\alpha_q}\int_{-\infty}^{+\infty} e^{-s_q(t_0+r'_*)}\psi_q(r'_*) \times[s_q\psi_0(r'_*)+v_0(r'_*)]dr'_*\ . \tag{52}$$

A. Response from compact sources

If ψ_0 and v_0 are reasonably smooth, and nonzero only if the Schwarzschild coordinate r lies on the compact interval $r_1<r<r_2$ where r_1 and r_2 are both finite and bounded away from $r=1$, the integral for the C_q is

$$C_q=\frac{A_{\mathrm{out}}(s_q)}{2s_q\alpha_q}\int_{r_1}^{r_2} e^{-s_q(t_0+r')}\psi_q(r')[s_q\psi_0(r')+v_0(r')] \times(r'-1)^{-s_q-1}r'dr'\ . \tag{53}$$

This compact source integral is finite, and can be evaluated numerically on the real r axis, as was demonstrated in Fig. 2. The late-time response may also be simply calculated. Equation (45) allows the last of integrals (47) to be evaluated to give the compact source radiative decay tail for $t-t_0\gg r_*-r'_*$ and $(t-t_0-r_*+r'_*)/r_*\ll 1$ as

$$\Psi_B(r_*,t)\sim\frac{(-)^l}{(2l+1)!!}[(l+2)!I(\psi_0)(t-t_0-r_*)^{-l-3}-(l+1)!I(v_0)(t-t_0-r_*)^{-l-2}]\ , \tag{54}$$

where the integrals $I(f(r))$ are given by

$$I(f)=\int_{r_1}^{r_2}(r')^{l+1}f(r')(r'-1)^{-1}r'dr'\ . \tag{55}$$

At very late times, $(t-t_0)/r'_*\gg 1$ and $(t-t_0)/r_*\gg 1$, Eq. (46) gives

$$\Psi_B(r_*,t)\sim\frac{2(-)^l}{[(2l+1)!!]^2}r^{l+1}[(2l+3)!I(\psi_0)(t-t_0)^{-2l-4}-(2l+2)!I(v_0)(t-t_0)^{-2l-3}]\ , \tag{56}$$

where the integrals $I(f)$ are the same as in Eq. (55). The tail that this last expression predicts for the $\psi_0(r)=\pi^{-1/2}\exp[-(r-r_0)^2]$ source is shown as part of Fig. 5, below.

B. Response from analytic sources

Physically "meaningful" initial-value source functions ψ_0 and v_0, to the extent that any purely initial-value problem is meaningful in black-hole physics, are analytic in r_*. They usually remain nonzero but finite as $r_*\to-\infty$, and typically fall off as r^{-l} and r^{-l-1}, respectively, as $r_*\to+\infty$. The quasinormal mode function $e^{-s_q r'_*}\psi_q(r'_*)$ diverges exponentially at both points. The resulting convergence problem for integral (52) can be solved by expanding the initial-condition functions in series of the form

$$\psi_0(r)=\sum_{j=1}^{\infty} c_j r^{-k_{1j}}(r-1)^{-k_{2j}}e^{-\sigma_{1j}(r-1)}\ , \tag{57}$$

$$v_0(r)=\sum_{j=1}^{\infty} d_j r^{-k_{3j}}(r-1)^{-k_{4j}}e^{-\sigma_{3j}(r-1)} . \tag{58}$$

Although it will usually be the case that $k_{1j}+k_{2j}$ is greater than or equal to the multipole moment l, that $k_{3j}+k_{4j}$ is greater than or equal to $l+1$, and that $\mathrm{Re}(\sigma_{ij})$ is positive or zero, no such restrictions are formally required by the following developments, and the exponents k_{ij} and σ_{ij} may be assigned whatever complex values are most convenient to the physics being considered. With these expansions Eq. (52) gives the excitation coefficients for the quasinormal modes as

$$C_q=\frac{A_{\mathrm{out}}(s_q)e^{-s_q t_0}}{2s_q\alpha_q}\sum_{j=1}^{\infty}[c_j s_q P_q(k_{1j},k_{2j},\sigma_{1j}) + d_j P_q(k_{3j},k_{4j},\sigma_{3j})] , \tag{59}$$

where the integrals $P_q(k_1,k_2,\sigma)$ are given by

$$P_q(k_1,k_2,\sigma)=\int_{-\infty}^{\infty} e^{-s_q r_*-\sigma(r-1)} \times\psi_q(r_*)r^{-k_1}(r-1)^{-k_2}dr_* . \tag{60}$$

This integral is but a formal expression for the $P_q(k)$, since $\mathrm{Re}(s_q)<0$ and $\mathrm{Re}(\sigma)$ frequently vanishes. In fact, since $\mathrm{Re}(s_q)\to-\infty$ as $q\to\infty$, for *any* σ there will be a minimum q for which the integrand diverges as $r_*\to\pm\infty$ along the real r_* axis. However, the analyticity of the integrand in r_* is the key property that allows integral (60) to be evaluated despite this formal divergence. If one considers $r_*=+\infty$ and $r_*=-\infty$ to be, in the Riemannian sense, the same point, then by Cauchy's theorem there is no reason to constrain the integration contour to real values of r_*. All that is required is that the contour begin and end at the point $r_*=\infty$, and that on the contour the integral be nonzero and finite. Equation (26) defines $\psi_q(r_*)$ in terms of the Schwarzschild coordinate r, and allows us to write

$$P_q(k_1,k_2,\sigma)=e^{s_q}A_{\mathrm{out}}{}^{-1}(s_q)\sum_{n=0}^{\infty}\left[a_n(s_q)\oint_C e^{-(s_q+\sigma)(r-1)}r^{1-n-k_1-2s_q}(r-1)^{n+s_q-k_2-1}dr\right] , \tag{61}$$

where the contour C must be chosen to include the points $r=1$ and $r=\infty$. The integrand in this expression is singular at $r=1$ for $n-k_2\le-\mathrm{Re}(s_q)$, and usually is also singular as $r\to\infty$ along the real r axis. However, the branch point at $r=1$ allows the integral to be evaluated term by term on the contour C illustrated in Fig. 3.

With the variable change $u=(s_q+\sigma)(r-1)$, the integrals in Eq. (61) for $P_q(k_1,k_2,\sigma)$ become

$$P_q(k_1,k_2,\sigma)=e^{s_q}A_{\mathrm{out}}{}^{-1}(s_q)\sum_{n=0}^{\infty}\left[a_n(s_q)(s_q+\sigma)^{k_2-n-s_q}\oint_F e^{-u}u^{n+s_q-k_2-1}[1+u/(s_q+\sigma)]^{1-n-k_1-k_2-2s_q}du\right] , \tag{62}$$

where the contour C for the original variable r becomes, for the new variable u, the contour F illustrated by Morse and Feshbach's[30] Fig. 5.12, and those authors Eq. (5.3.52) then yields the immediate solution

$$P_q(k_1,k_2,\sigma)=e^{s_q}A_{\mathrm{out}}{}^{-1}(s_q)\sum_{n=0}^{\infty}a_n(s_q)\Gamma(n+s_q-k_2)e^{-i\pi(n-k_2+s_q)}U_2(n+s_q-k_2\,|\,2-k_1-k_2-s_q\,|\,s_q+\sigma) . \tag{63}$$

The irregular confluent hypergeometric function $U_2(a\,|\,c\,|\,z)$ defined by Morse and Feshbach is related to the more commonly used $U(a,c,z)$ defined by Slater[31] by $U_2(a\,|\,c\,|\,z)=e^{i\pi a}U(a,c,z)$, so that the ultimate expression for the coefficient $P_q(k_1,k_2)$ becomes[32]

$$P_q(k_1,k_2,\sigma)=e^{s_q}A_{\mathrm{out}}{}^{-1}(s_q)\sum_{n=0}^{\infty}a_n(s_q)\Gamma(n+s_q-k_2)U(n+s_q-k_2,2-k_1-k_2-s_q,s_q+\sigma) . \tag{64}$$

The coefficients $a_n(s_q)$ are minimal solutions of the recurrence relation (A3), and $U(a+n,b,c)$ are minimal solutions of Slater's equation (13.4.15). Proof of the convergence of series of the form (64) is given in Appendix C of paper II. The confluent hypergeometric functions can be generated from Slater's[31] equations (13.1.2), (13.1.3), and (13.4.15), while the complex γ-function evaluation is discussed by Kuki.[33] The validity of expressions (59) and (64) is illustrated by Fig. 4, where only the c_1 term was used in the series and σ_{11} was zero. Similar calculations have been done retaining more terms in the series (59), and using complex values for the σ and k's.

C. The branch-cut contribution and late-time decay tails

The branch-cut contribution $\Psi_B(r_*,t)$ due to the analytic source (57) and (58) can be evaluated at late times by integrating

$$\Psi_B(r_*,t)=\int\int G_B(r_*,t\,|\,r'_*,t')Q(r'_*,t')dr'_*dt' =-2\sum_{j=1}^{\infty}\left[c_j\int_0^{-\infty}e^{s(t-t_0)}sF_l(-is,isr)I_0(k_{1j},k_{2j},\sigma_{1j},l,s)ds+d_j\int_0^{-\infty}e^{s(t-t_0)}F_l(-is,isr)I_0(k_{3j},k_{4j},\sigma_{3j},l,s)ds\right] , \tag{65}$$

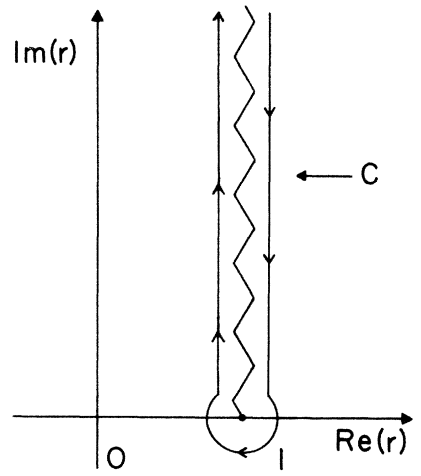

FIG. 3. Contour C for the evaluation of the quasinormal mode excitation coefficient $P_q(k)$ of Eq. (61). This contour is to be used when $\mathrm{Im}(s_q+\sigma)<0$. The contour used when $\mathrm{Im}(s_q+\sigma)>0$, as is usually the case for the complex-conjugate frequencies $\bar{s}_q$, is obtained by reflecting the contour C through the real r axis. Deformations of this contour are useful for a wide variety of excitation problems.

where the integrals $I_0(k_1,k_2,\sigma,l,s)$ are given, for $|s|\ll 1$, by

$$\lim_{s\to 0} I_0(k_1,k_2,\sigma,l,s) \sim \int_1^\infty e^{-\sigma(r-1)} r^{1-s-k_1}(r-1)^{s-1-k_2} F_l(-is,isr)\,dr \ . \tag{66}$$

Evaluation of these integrals is more difficult than their simple appearance would suggest, but Gradshteyn and Ryzhik's equations (6.563) and (6.569), at the small s limit for the Coulomb wave function F_l in Eq. (66), are helpful. For the important case when $k_1=l$, $k_2=0$, and $\sigma=0$ they yield

$$\lim_{s\to 0} I_0(l,0,0,l,s) \sim \frac{(is)^{l-1}}{(2l-1)!!} \ . \tag{67}$$

This result is fairly limited, but it does allow us to evaluate expression (65) for the important case when $\psi_0=r^{-l}$ and $v_0=0$ in two distinct asymptotic regions in time.

(1) $(t-t_0-r_*)\gg 1$ but $(t-t_0-r_*)/r_* \ll 1$. In this radiation region the magnitudes of $|sr_*|$ that contribute to the integrals are very large, the Coulomb wave functions may be approximated by $F_l(-is,isr) \sim (\frac{1}{2})\exp[-sr_*-(l+1)i\pi/2]$, and the branch-cut contribution by

$$\Psi_B(r_*,t) \sim \frac{(-)^{l+1} l!}{(2l-1)!!}(t-t_0-r_*)^{-l-1} \ . \tag{68}$$

This radiating decay tail represents a new and heretofore unsuspected feature in radiation effects from black holes. The investigation of the $(t-t_0)/r_* \gg 1$ region discussed next suggests that a small correction must probably be made to these coefficients when the source field $\Psi(r,t)_{t=0}$ has the more physically reasonable form $\psi_0=r^{-l}\sum_{n=0}^{\infty} a_n r^{-n}$ (with $a_0=1$).[34] It should be noted that, for $l=2$, the magnitude of this decay tail becomes comparable in magnitude to the ringing of the fundamental quasinormal mode only for $t-t_0-r_*\sim 75$, at which time the magnitude is less than than 10^{-5} of its value at the onset of the quasinormal ringing.

(2) $r_*>1$ and $(t-t_0)/r_* \gg 1$. In this very-late-time region the only s that will contribute to the integrals in (65) are so small that $|sr_*| \ll 1$ and $F_l(-is,isr) \sim (isr)^{l+1}/(2l+1)!!$. In this case

$$\Psi_B(r_*,t) \sim (-)^{l+1} 2r^{l+1}(2l)!! \frac{(t-t_0)^{-2l-2}}{(2l-1)!!} \ . \tag{69}$$

This very-late-time nonradiating tail was first described by Price,[15] and expression (69) is identical to Cunningham, Price, and Moncrief's[16] Eqs. (IV.1) and (IV.2). Numerical experiments (Fig. 5) suggest that initial sources $\psi_0=r^{-k}$ for $k=l+1$ and $k=l+2$ will also produce $(t-t_0)^{-2l-2}$ decay tails, but of somewhat smaller magnitude. The hypergeometric source function relevant to stellar collapse problems[16] (see Sec. IV below) contains such higher-order terms, so these minor corrections will be of some physical significance. It is interesting that the sign of expressions (68) and (69) for the tails from the analytic sources differs from the sign of expressions (54) and (55) for the tails from the compact sources.

Figure 5 shows log-log plots of the function $\Psi_B(r,t)$ for electric dipole fields, as measured by an observer at $r=10$, with $t_0=0$; the time interval is $20<t<50$, which is moderately late compared to r. The curves plot the logarithm of the magnitude of the difference between the total time response, as obtained by integrating the initially stationary source fields $\Psi(r,t)_{t=0}$ forward in time by the method of characteristics, and the contribution from the first four quasinormal modes as given by expression (59). The curves are labeled by the functional form of the perturbing source field. The r^{-k} curves were computed from expression (59) with $c_1=1$, $c_2=0$, $l=1$, and $k_1=1$, 2, and 3. Each of these curves has the same slope at $t=50$, namely, $\partial \log\Psi(r,t)/\partial \log t\,|_{r=10,t=50}\simeq -4.5$, which suggests that the components of an initially stationary source field that fall off as r^{-k}, for $k=l$, $k=l+1$, and $k=l+2$, may also contribute to the final $(t-t_0-r_*)^{-l-1}$ decay tail. This difference plot provides a valuable check on the predictions of Eq. (69), and allows another method of estimating the small s limiting value of the integral $I_0(k,l,s)$, Eq. (66), for $k>l$. For the present I attribute the deviation of the slopes of these curves from the predicted value -4 to the relatively short times over which they are plotted: $(t-t_0)/r=5$ at the last point on the interval. The form of the late-time response from noncompact source fields which fall off faster than r^{-l-2} remains to be established.

The astrophysical conditions that prevail for the radiative decay tails, which correspond to a distance in light-seconds between the black hole and the observer that is much longer than the time period of the radiation events, is more difficult to study numerically than is the very-late-time regime of the nonradiating decay tails, and is deferred to the next section. The present derivation of the radiative expressions (54) and (68) differs from that for

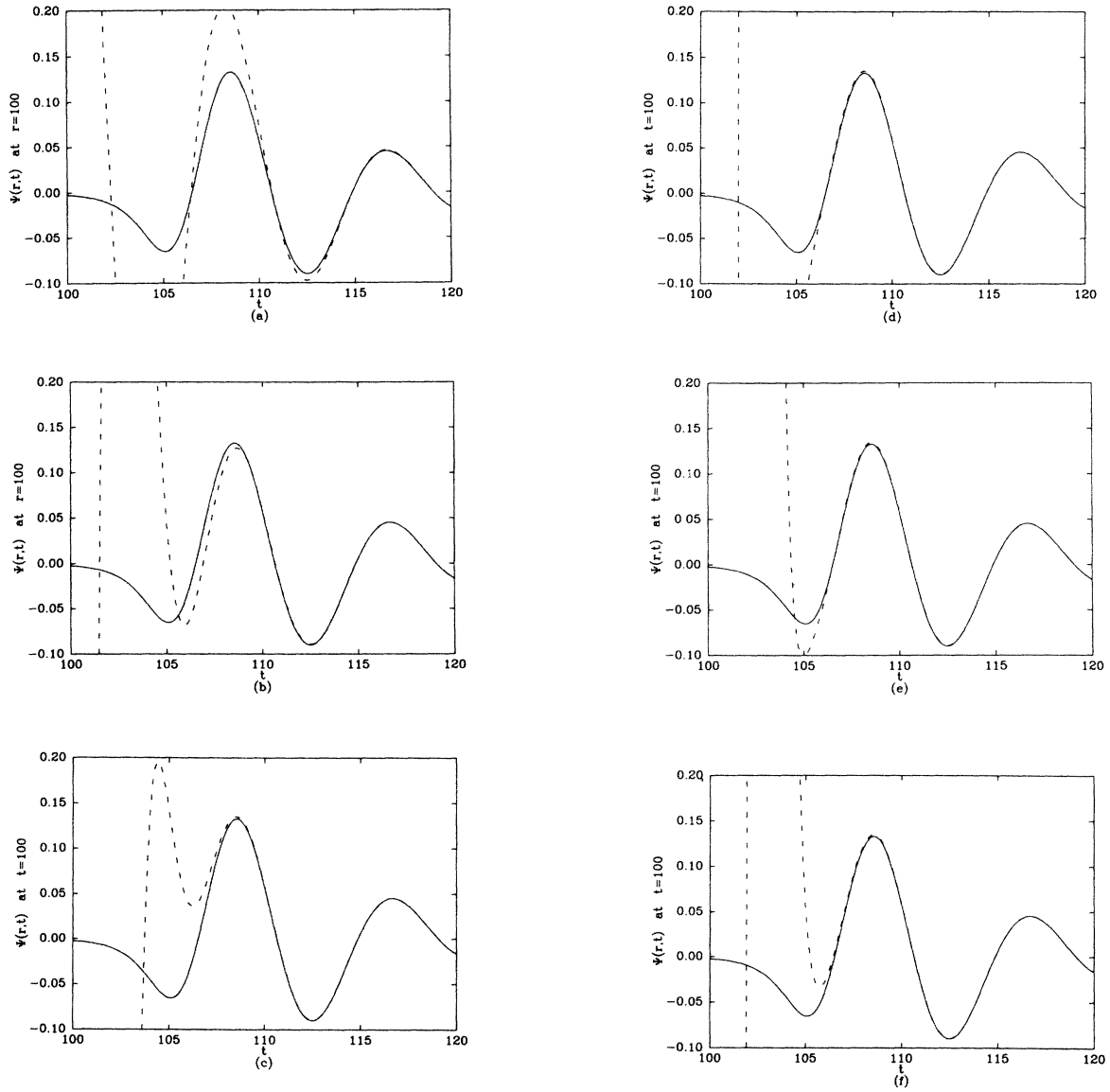

FIG. 4. Excitation of the first six $l=2$ gravitational Schwarzschild quasinormal modes resulting from a stationary initial perturbation $\Psi(r,t=0)=r^{-2}$, as seen by an observer at $r=100$. The dashed curves are the sum of quasinormal mode contributions, and were obtained by evaluating expansion (59) with $c_1=1$, $c_2=0$, $k_1=l=2$, and $q=1,2,\ldots,6$. Only the fundamental term $q=1$ was retained in (a); the first two terms $q=1,2$ were retained in (b); the first three terms in (c), etc. The solid curve is the total response due to this perturbation as obtained by numerical integration, via the method of characteristics, of Eq. (1) with $q(r_*,t)=r^{-2}\delta'(t)$. The step size for the numerical integration was $\Delta r_*=\Delta t=0.0125$.

the very-late-time nonradiative result (69) only in the limit in which one evaluates the Coulomb wave function $F_l(is,-isr)$. This is a very simple generalization, and unifies the two decay-tail results in a most elegant fashion.

IV. THE CHARACTERISTIC-VALUE PROBLEM AND RADIATION FROM COLLAPSING STARS

A generalization of the initial-value problem discussed in Sec. III is the problem of mixed Cauchy and characteristic data. The Green's-function integrals that propagate such mixed data are derived in Appendix B, the results of which are used here to compute the excitation of the quasinormal ringing. An astrophysically interesting example of quasinormal ringing from a characteristic-value problem is offered by the work of Cunningham, Price, and Moncrief,[16–18] who followed the gravitational radiation emitted during the collapse, via the Oppenheimer-Snyder model, of a massive star. I recapitulate their approach.

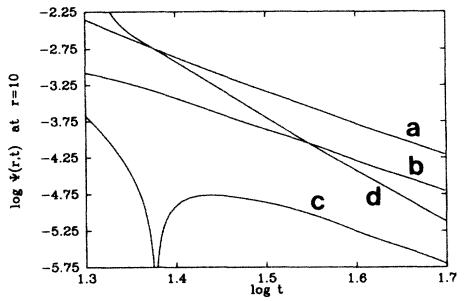

FIG. 5. Log-log (base 10) plot of the function $\Psi_B(r,t)$ for electric dipole fields as a function of t, as measured by an observer at $r=10$. The curves are the difference between the total time response, obtained by integrating the initially stationary source fields, $\Psi(r,t)_{t=0}$, forward in time by the method of characteristics, and subtracting the contribution from the first four quasinormal modes as given by expressions (48) and (59). The curves are labeled according to the source field as a, $\Psi(r,t)_{t=0}=r^{-1}$; b, $\Psi(r,t)_{t=0}=r^{-2}$; c, $\Psi(r,t)_{t=0}=r^{-3}$; d, $\Psi(r,t)_{t=0}=\pi^{-1/2}\exp[-(r'-5)^2]$. The response from the Gaussian source field was obtained by integrating expression (48) along the real r axis from $r=2$ to 8. The slope of this curve at $t=50$ is $\partial\log\Psi(r,t)/\partial\log t\,|_{r=10,t=50}=-6.3$, which is within $r/t\sim 20\%$ of the predicted value of -6.

The star is assumed to be in equilibrium prior to the onset of collapse at $t=0$, and the evolution of radiation in the region exterior to the surface of the star is formulated in terms of the characteristic-value problem. Assume the stellar surface is initially at $r_*=-u_0$ at $t=0$. Reference 16 deals with axial perturbations and, the sources being interior to the surface, the value of Ψ and its derivative on the $t-r_*=u_0$ characteristic is taken to be the static solution to the wave equation (1):

$$\left[\frac{\partial^2}{\partial r_*^{\,2}}\Psi(r_*,t) - \frac{r-1}{r^3}\left[l(l+1)-\frac{3}{r}\right]\Psi(r_*,t)\right]_{t-r_*=u_0}=0\,. \quad (70)$$

The solution that is regular as $r_*\to\infty$ is simply

$$\Psi(r,t)\,|_{t-r_*=u_0}=q_l r^{-l}\,{}_2F_1(l-1,l+3;2l+2;1/r)\,, \quad (71)$$

where ${}_2F_1(a,b;c;z)$ is the hypergeometric function that is regular as $z\to 0$. Here q_l is a scaling parameter that reflects the strength of the perturbation, and is obtained from the junction conditions on the exterior solution to the wave equation with the solution interior to the star. Since the data on the $u=u_0$ characteristic is that of a field that was initially stationary on the $t=0$ hypersurface, this characteristic-value problem shares some of the aspects of the initial-value problem discussed in the previous section, and in particular will be seen to possess the same radiative decay tails arising from the frequency-domain branch cut.

In terms of the characteristic coordinates $v=t+r_*$ and $u=t-r_*$, the world line of the stellar surface asymptotically approaches an ingoing null ray $t+r_*=v_1$ as the surface falls through the horizon. Price[15] has shown that the asymptotic form of the data on this characteristic must approach $a+b\exp(-\frac{1}{2}u)$ as $u\to\infty$. The value of v_1, the magnitudes of the constants a and b, and the way in which Ψ approaches this asymptotic form, are determined by the details of the collapse. Cunningham, Price, and Moncrief determined the value of Ψ on the $v=v_1$ characteristic by numerically integrating the interior wave equation for density perturbations during Oppenheimer-Snyder collapse outward to the stellar surface, changing coordinates, and continuing the integration out to the $v=v_1$ characteristic. They found that, apart from determining the magnitude q_l of the external perturbation, "the dynamics of the field in the interior of the star plays an unimportant role in determining the exterior radiation."

The characteristics are diagramed in Fig. 6. In the following example I will approximate the value of Ψ on the $t=r_*=v_1$ characteristics by the explicit function

$$\Psi(r,t)\,|_{t+r_*=v_1}=a+b(1-1/r)+c(1-1/r)^2\,, \quad (72)$$

which approaches $a+b\,e^{r_*}$ in the limit as $r_*\to-\infty$. This simple form is suggested by the shape of the topmost boundary of Cunningham, Price, and Moncrief's[16] Fig. 3. It should be noted that this form has been chosen only as an example of how these calculations might proceed. More terms, perhaps involving other functional forms such as damped or undamped sinusoids, can always be added to series (72) in order for it to more accurately match the conditions on the $v=v_1$ characteristic as determined by some other method of calculation. Alternatively, a relatively simple form such as the one shown might be retained, with the values of q_l, a, and v_1 chosen to match those generated in a more detailed model. The difference function between the detailed and the simple models will then be compact, and easily dealt with numerically.

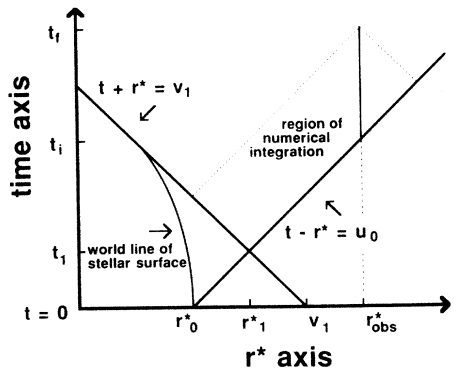

FIG. 6. Spacetime diagram for the simplified model problem approximating Oppenheimer-Snyder collapse from an initial radius r_0. The world line of the stellar surface asymptotically approaches the $v=v_1$ characteristic as the collapse progresses. The value of the metric perturbation, $\Psi(u,v)_{v=v_1}$, is given on this characteristic by Eq. (72). The corresponding value on the $u=u_0=-r_0^*$ characteristic is given by Eq. (71). The time response at $r_*=r_{\rm obs}^*$ is then found by integrating Eq. (1) within the rectangular region bounded by the dashed lines and the $u=u_0$ and $v=v_1$ characteristics.

Cunningham, Moncreif, and Price's results show that for the Oppenheimer-Snyder model of stellar collapse the value of the initially static gravitational perturbation, as measured at the surface of the star, increases smoothly and stays within $\pm 20\%$ of r_0/r as the surface collapses through the horizon.[35] Using the median value and Eq. (71), the parameter a in Eq. (72) is therefore chosen to be

$$a = q_l r_0^{-l+1} {}_2F_1(l-1,l+3;2l+2;1/r_0) . \tag{73}$$

The parameters b and c are then chosen such that $\Psi(r_*,t)$ on the $t+r_*=v_1$ characteristic smoothly matches $\Psi(r_*,t)$ on the $t-r_*=u_0$ characteristic at the point the two characteristics intersect:

$$a+b(1-1/r_1)+c(1-1/r_1)^2 = q_l r_1^{-l} {}_2F_1(l-1,l+3;2l+2;1/r_1) , \tag{74}$$

$$\frac{d}{dr}[b(1-1/r)+c(1-1/r)^2]\bigg|_{r=r_1} = \frac{d}{dr}[q_l r^{-l} {}_2F_1(l-1,l+3;2l+2;1/r)]\bigg|_{r=r_1} . \tag{75}$$

It remains only to determine r_1^* from Fig. 6, and the value v_1 of the final ingoing characteristic.

Denote the radius of the collapsing Oppenheimer-Snyder star, in Schwarzchild's coordinate, by r_s, and let the collapse start from $r_s=r_0$ at $t=0$. The value of the ingoing characteristic v_1 is found by following the world line (r_s^*,t_s) of the stellar surface during the collapse, and determining the value of $T_s+r_s^*$ when the surface passes through the horizon. The horizon is at $r=2M$, which is scaled to $r=1$. Hence

$$v_1 = \lim_{r_s\to 1}(t_s+r_s^*) = \lim_{r_s\to 1}[t_s+r_s+\ln(r_s-1)] . \tag{76}$$

The Schwarzchild coordinates of the stellar surface, r_s and t_s, are parametrized by the cycloid coordinate η:

$$r_s(\eta)=r_0\cos^2(\eta/2) , \tag{77}$$

$$t_s(\eta)=\ln\left[\frac{(r_0-1)^{1/2}+\tan(\eta/2)}{(r_0-1)^{1/2}-\tan(\eta/2)}\right] +(r_0-1)^{1/2}[\eta+\tfrac{1}{2}r_0(\eta+\sin\eta)] . \tag{78}$$

The collapse starts at $\eta_0=0$, and the final singularity is encountered at $\eta_f=\pi$. The horizon is passed[36] at $\eta_1=2\cos^{-1}(r_0^{-1/2})$. Equations (76)–(78) yield

$$v_1 = \lim_{r_s\to 1}(t_s+r_s^*) = 1+\ln 4(1-r_0^{-1}) +(r_0-1)^{1/2}[\eta_1+\tfrac{1}{2}r_0(\eta_1+\sin\eta_1)] , \tag{79}$$

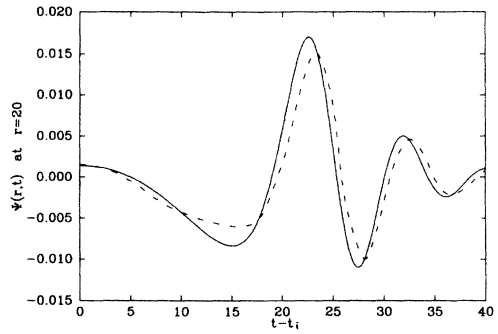

FIG. 7. Comparison of the result of integrating the approximate model with the full Oppenheimer-Snyder result as published by Cunningham, Price, and Moncrief (Ref. 17). The initial radius was taken to be $r_0=8M$. The dashed curve is a reproduction of the dashed curve in Moncrief, Cunningham, and Price's (Ref. 19) Fig. 1 (values furnished courtesy of R. H. Price). The solid curve is the result of integrating the simplified model problem.

and the simplified model problem is then specified as follows: (1) Choose a radius r_0 from which to begin the collapse, and a perturbation magnitude q_l; (2) compute v_1 from (79); (3) from Fig. 6, find $r_1^*=\frac{1}{2}(v_1+r_0^*)$, and $t_1=\frac{1}{2}(v_1-r_0^*)$; (4) specify the data everywhere on the "first ray" $t-r_*=u_0=-r_0^*$ by Eq. (71); (5) choose the constants a, b, and c in Eq. (72) to satisfy Eqs. (73), (74), and (75); (6) integrate, via the method of characteristics, the solution $\Psi(r_*,t)$ up to the observer's position at $r_{\rm obs}^*$ for times between $t=r_{\rm obs}^*-r_0^*$ and $t=t_0$.

The waveform resulting from this simplified model is compared with that produced by exact Oppenheimer-Snyder collapse in Fig. 7. The two waveforms have, for the present purposes, their essential features in common.

Excitation coefficients for the quasinormal modes

The response for this model problem is obtained from Eq. (B7) with $Q(u,v)=0$, $\kappa=1$, $u_0=-r_1^*$, and $v_0=v_1=+r_1^*$:

$$\Psi(u,v)=2\int_{-r_1^*}^{\infty} G(u,v\mid u',v_1)\Psi_{,u'}(u',v_1)du' -2\int_{r_1^*}^{\infty} G_{,v'}(u,v\mid u_0,v')\Psi(u_0,v')dv' . \tag{80}$$

Note that the v_1 illustrated in Fig. 6 is equivalent to the v_0 used in Fig. 11. The functions $\Psi(u,v)$ and $G(u,v\mid u',v')$ are exactly the same as when expressed explicitly in terms of r_* and t, and expressions (17) and (18) allow ready evaluation of G and its derivatives. In this particular example, however, Ψ is specified in closed form on the boundary characteristics $u=u_0$ and $v=v_1$, and hence is slightly easier to manipulate than is expression (27) for G_Q. It is therefore convenient to integrate the second integral once by parts and cast the derivative on Ψ to obtain

$$\Psi(u,v)=2G(u,v\mid u_0,v_1)\Psi(u_0,v_1)+2\int_{-r_1^*}^{\infty}G(u,v\mid u',v_1)\Psi_{,u'}(u',v_1)du'+2\int_{r_1^*}^{\infty}G(u,v\mid u_0,v')\Psi_{,v'}(u_0,v')dv' , \quad (81)$$

where causality has required that the first term's contribution at $v=\infty$ vanish. In other problems, where values of Ψ on the boundary characteristics might be obtainable only through numerical calculation of a more complicated collapse process, it may be preferable to cast all the derivatives on G. Either way, the integrals in (81) are expressed in terms of the r_*,t coordinates using the derivative relations

$$\frac{d}{du}=\frac{1}{2}\left[\frac{\partial}{\partial t}-\frac{\partial}{\partial r_*}\right], \quad \frac{d}{dv}=\frac{1}{2}\left[\frac{\partial}{\partial t}+\frac{\partial}{\partial r_*}\right] . \quad (82)$$

In the direction of the $u=-r^*_{\rm obs}$ and $v=v_1$ characteristics, the differentials du and dv are related to dr_* by

$$dv=2dr_*, \quad du=-2dr_* . \quad (83)$$

Further, the time derivative of our particular data function Ψ, given by Eqs. (71) and (72), vanishes on both these characteristics, so that

$$\Psi(r_*,t)=2G(r_*,t\mid r_1^*,t_1)\Psi(r_1^*,t_1)+2\left[\int_{r_1^*}^{\infty}G(r_*,t\mid r'_*,t')\Psi_{,r_*}(r'_*,t')dr'_*\right]_{t'=r'_*-r_1^*}+2\left[\int_{r_1^*}^{-\infty}G(r_*,t\mid r'_*,t')\Psi_{,r_*}(r'_*,t')dr'_*\right]_{t'=r_1^*-r'_*} . \quad (84)$$

The excitation coefficients for the quasinormal modes are found by substituting G_Q of Eq. (27) into the integrals of (84). The ringing portion Ψ_Q of the response function $\Psi(r_*,t)$ can then be expressed as in Eq. (49) by

$$\Psi_Q(r_*,t)=2\,\mathrm{Re}\left[\sum_{q=1}^{\infty}C_q\psi_q(r_*)e^{s_q(t-r_*)}\right] , \quad (85)$$

where, for the present characteristic data problem, the excitation coefficients are given by

$$C_q=\frac{A_{\rm out}(s_q)}{s_q\alpha_q}\left[\Psi(r_1,t_1)\psi_q(r_1)e^{-s_qr_1}+e^{-s_qr_1}\left[\int_{r_1}^{1}\Psi_{,r'}(r',t')\psi_q(r')dr'\right]_{t'=r_1^*-r'_*}+e^{s_qr_1}\left[\int_{r_1}^{\infty}\Psi_{,r'}(r',t')\psi_q(r')e^{-2s_qr'_*}dr'\right]_{t'=r'_*-r_1^*}\right] . \quad (86)$$

The value of $\Psi(r',t')_{t'=r_1^*-r'_*}$ on the $v=v_1$ characteristic for the first integral is given by Eq. (72), and its value on the $u=u_0$ characteristic for the second integral by Eq. (71). The integrals in Eq. (86) do not converge on the real r axis, and contours must be chosen such that the contributions at $r=1$ and ∞ vanish. In terms of the contours C_1 and C_2 of Fig. 8, the excitation coefficients are finally obtained by

$$C_q=\frac{A_{\rm out}(s_q)}{s_q\alpha_q}\left[\Psi(r_1,t_1)\psi_q(r_1)e^{-s_qr_1}-e^{-s_qr_1}(1-e^{4\pi is_q})^{-1}\int_{C_1}\Psi_{,r'}(r',t')\psi_q(r')dr'\mid_{t'=r_1^*-r'_*}+e^{s_qr_1}\int_{C_2}\Psi_{,r'}(r',t')\psi_q(r')e^{-2s_qr'_*}dr'\mid_{t'=r'_*-r_1^*}\right] . \quad (87)$$

As stressed previously, the analytic behavior of Ψ on the source characteristics, $u=u_0$ and $v=v_1$ as $u\to\infty$ and $v\to\infty$, is needed in order to evaluate the integrals. As Cunningham, Price, and Moncrief have shown however, this information is readily approximated. The factor $(1-e^{4\pi is_q})^{-1}$ comes from the integral around the branch point $r=1$ in Fig. 8(a), and is required if the integral is to reduce to the "correct" expression (87) in the limit the data $\Psi_{,r'}$ has compact support.

The integrals in Eq. (87) are readily evaluated numerically. The hypergeometric function ${}_2F_1(a,b;c;z)$ was generated by the Chebyshev expansion subroutines CCOEF2 and EVAL given by Luke,[38] and checked by the rational approximation subroutine R2F1 of the same author. The quasinormal mode functions $\psi_q(r)$ were generated by the algorithm explained in the present Appendix A. As a check on the equivalence of this contour method with the method of subtracting divergences used by Detweiler and Szedenits,[5] the first of the integrals in (86) was evaluated independently as

$$(1-e^{4\pi is_q})^{-1}\int_{C_1}\Psi_{,r'}(r',t')\psi_q(r')dr'\mid_{t'=r_1^*-r'_*}=\int_1^{r_1}[\Psi_{,r'}(r',t')\psi_q(r')-f(r')]_{t'=r_1^*-r'_*}dr'+F(r)_{r=r_1} , \quad (88)$$

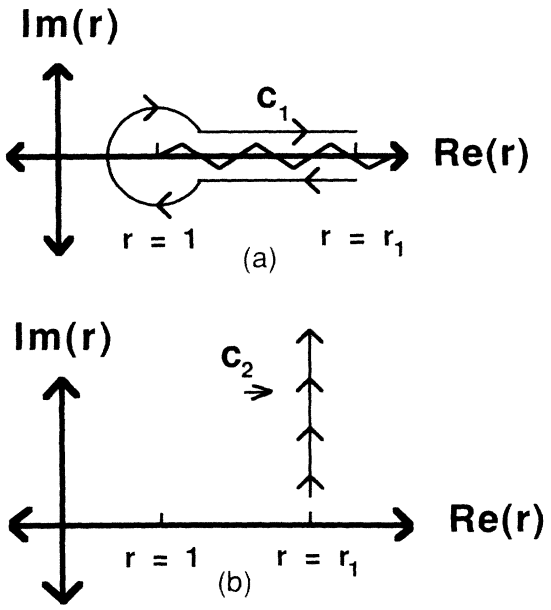

FIG. 8. Contours for determining the quasinormal mode excitation for the characteristic value problem. Contour C_1 is used for the Schwarzschild r coordinate integration of the $v=v_1$ characteristic, Eq. (87). It begins and ends on opposite sides of the branch cut at $r=r_1$. Contour C_2 goes from r_1 to imaginary infinity, where the second of the integrands in (87) will converge since $\mathrm{Im}(s_q)<0$: the contour must be inverted for the complex-conjugate frequencies $\bar{s}_q$.

where $F(r)=\int f(r)dr$, and $f(r)$ was chosen to cancel the singularity of $\Psi_{,r'}(r',t')\psi_q(r)$ at $r=1$. This was done by taking f to be the first two terms in the Taylor-series expansion for $\Psi_{,r}(r,t)_{t=r_1^*-r_*}\psi_q(r)$ about $r=1$, which is another way of using the analytic information about Ψ on the source characteristic near that point. The integrand on the right-hand side of (88) is then finite at $r=1$ for the lowest-order frequencies s_1 and s_2, and the integration can proceed along the real r axis between $r=1$ and $r=r_1$. This result agrees with the contour integral on the left-hand side of (88) to within the truncation error of six decimal places.[39] Results of Eqs. (85)–(87) are shown in Fig. 9(a), where the result of numerically integrating the model problem of collapse starting from $r_0^*=4$ is compared with the excitation due to the first four quasinormal modes. A log-log plot of the difference between these two curves, demonstrating the late-time radiative decay tail predicted in Sec. III, is shown in Fig. 9(b). A detailed analysis of the response from this (and other) collapse models could be presented along the same lines as the six time-region discussion of the impulse response given in Sec. II. However, the time-evolution of the geometry during supernova is extensive enough that only those elements occurring relatively late in the collapse are amenable to analysis by simple perturbation theory: these will be characterizable by their excitation of the underdamped quasinormal modes, and of the late-time decay tails.

V. THE RADIAL IN-FALL PROBLEM AND THE RESPONSE FROM SOURCES EXTENDED IN BOTH SPACE AND TIME

The explicit expansion (27) for the quasinormal mode component $G_Q(r_*,t\mid r'_*,t')$ of the time domain Green's function $G(r_*,t\mid r'_*,t')$ in principle allows one to determine the quasinormal mode excitation due to an arbitrary source $Q(r_*,t)$. Convergence of the double integral (50) for the expansion coefficients C_q may create difficulties, although none that are insurmountable provided one has an analytic representation for Q in the limits as r_* and t go to $\pm\infty$. If one has such an asymptotic representation for Q, and numeric values (for real r_* and t) over a finite range connecting the asymptotic limits, then the integrals (50) may be evaluated numerically on the finite range, and the divergences at the end points eliminated by finishing

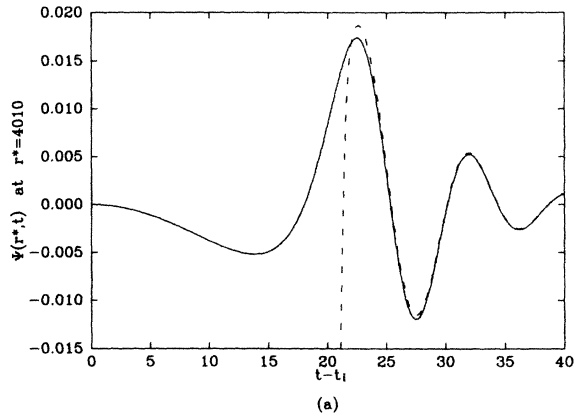

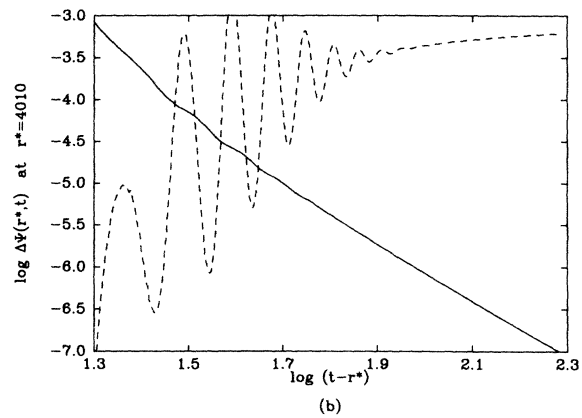

FIG. 9. Comparison of the quasinormal mode response for the simplified model collapse problem with the total response as determined by direct integration of the wave equation. The solid curve in (a) is the same as in Fig. 7, while the dashed curve represents the contribution of the first six quasinormal modes. The pattern of the contribution from successive modes is similar to that shown in Fig. 4. The collapse was started at $r_0=8M$, and the observer was placed at $r=4002.25$. The solid curve in (b) is a log-log (base 10) plot of the difference between the two curves in (a), demonstrating the late-time radiating decay tail discussed in Sec. III. The dashed curve is the derivative of this logarithmic difference, and shows how the tail slowly approaches the predicted $-\frac{2}{3}(t-r^*_{\mathrm{obs}})^{-3}$ behavior.

the integrals at $\pm\infty$, either numerically or analytically, on a path for which the integrals converge. The order in which the integrations are done, and the contours used, will naturally be determined by the ease in which the quantities involved can be evaluated, and will depend on the particular problem being considered.

For temporally extended sources it will frequently be convenient to write the integrals for the response function as

$$\Psi(r_*,t)=\int_{-\infty}^{\infty}\int_{-\infty}^{\infty}G(r_*,t\mid r'_*,t')Q(r'_*,t')dr'_*dt' =\frac{1}{2\pi i}\int_{\epsilon-i\infty}^{\epsilon+i\infty}e^{st}\int_{-\infty}^{\infty}g(r_*,r'_*,s)q(r'_*,s)dr'_*ds\ , \tag{89}$$

where

$$q(r'_*,s)\equiv\int_{-\infty}^{+\infty}e^{-st'}Q(r'_*,t')dt'\ . \tag{90}$$

The excitation coefficients, as defined in Eq. (50), are then

$$C_q=\frac{A_{\rm out}(s_q)}{2s_q\alpha_q}\int_{-\infty}^{+\infty}\int_{-\infty}^{+\infty}e^{-s_q(t'+r'_*)}\psi_q(r'_*)Q(r'_*,t')\times dr'_*dt' \tag{91}$$

$$=\frac{A_{\rm out}(s_q)}{2s_q\alpha_q}\int_{-\infty}^{+\infty}e^{-s_qr'_*}\psi_q(r'_*)q(r'_*,s_q)dr'_* \tag{92}$$

$$=\frac{A_{\rm out}(s_q)}{2s_q\alpha_q}\int_C e^{-s_qr'}\psi_q(r')q(r',s_q)(r'-1)^{-s_q-1}r'dr'\ . \tag{93}$$

The frequency-domain source function $q(r'_*,s_q)$ may be thought of as the Fourier transform $\int_{-\infty}^{+\infty}e^{i\omega t'}Q(r'_*,t')dt'$, either analytically continued to $\omega=is_q$, or else integrated along a contour for which the integral converges. The spatial integral (93) will then remain, and may be evaluated on some suitably normalized deformation of the contour C of Fig. 3, of which the combination of contours C_1 and C_2 of Fig. 8 is an example. The approach to $r=\infty$ will depend on the analytic nature of Q as $r\to\infty$, while the difference across the branch cut and the integral around $r=1$ will depend on the behavior of $q(r,s_q)$ as $r\to1$.

A simplification may result if the integrand in (93) possesses a Taylor expansion about $r=1$:

$$\lim_{r\to1}e^{-s_qr}\psi_q^{(+)}(r)q(r,s_q)(r-1)^{-s_q-1}=\sum_{n=0}^{\infty}\xi_n(r-1)^{\zeta_q+n}\ , \tag{94}$$

where ζ_q will usually be some positive multiple of s_q. Since the integral along the contour C of the total derivative of any function $F(r)$ that vanishes as $r\to\infty$ is zero, the integrand of (93) can be made finite at $r=1$ by subtracting from it the (nonunique) function

$$f(r)=\frac{d}{dr}\left[\sum_{n=0}^{N}b_n\frac{(r-1)^{\zeta_q+n+1}}{\zeta_q+n+1}e^{-a(r-1)}\right]\ , \tag{95}$$

where N is greater than or equal to the largest integer in the real part of $-\zeta_q$, and a is any convenient complex constant. The coefficients b_n are related to the ξ_n by

$$b_0=\xi_0/(\zeta_q+1),\quad(\zeta_q+n+1)b_n-ab_{n-1}=\xi_n\ ,\quad n=1,2,\ldots,N\ , \tag{96}$$

and the integral (92) for the expansion coefficient can then be written

$$C_q=\frac{A_{\rm out}(s_q)}{2s_q\alpha_q}\int_{r=1}^{\infty}[e^{-s_qr}\psi_q(r)q(r,s_q)(r-1)^{-s_q-1}r -f(r)]dr\ . \tag{97}$$

The integration may proceed along the real values of r for which $q(r,s_q)$ can be generated numerically, and completed to $r=\infty$ on a convergent path using the requisite asymptotic knowledge of q as $r\to\infty$. Once again, however, the subtraction of a suitable total derivative can presumably cancel the large r divergence of the integrand, and lead to an integral for C_q that can be evaluated entirely on the real r axis.

The vanishing of the contribution of total derivatives has been used by Detweiler and Szedenits[5] in their study of the radiation emitted by a test particle spiraling into a black hole. In their Eq. (A7) these authors experienced similar convergence problems for source-term integrals, but rather than a discussion in terms of the contour of integration, Detweiler and Szedenits consider the freedom to subtract arbitrary total derivatives in the same aspect as integrations by parts, and interpret both in terms of the boundary conditions on the radiation problem: "It may be noticed that all surface terms from the integrations by parts leading to equation (A7) were dropped intentionally. This is allowed. Any nonvanishing surface term may be ultimately identified as an additional gravitational wave sent in from infinity or out of the black hole. By dropping all surface terms, we are effectively enforcing the boundary conditions: the waves must be outgoing at infinity and ingoing at the event horizon. To rectify the nonconvergence of the equation, we are now free to subtract from the integrand any vanishing or nonvanishing divergence."

More is said of surface terms and boundary conditions, in terms of characteristics, in Appendix B. It should be noted that the two methods, the subtracting of derivatives and the deforming of integration contours, both require the same analytic information about the source-term integrand. I illustrate the equivalence of the two procedures by considering quasinormal mode excitation in the small body radial in-fall problem.

The radial in-fall problem

The problem of determining the gravitational radiation emitted by a small test particle falling radially into a Schwarzschild black hole was first formulated by Zerilli,[12] and solved by Davis, Ruffini, Press, Price, and Tiomno,[1,2]

who computed the total radiation emitted by numerically evaluating the Green's function for real frequencies. The more general problem of spiral in-fall was subsequently solved by Detweiler and Szedenits,[5] who used the Newman-Penrose formalism.

Here I retain Zerilli's formalism and look at the simplest case where the test particle is initially at rest at spatial infinity in the distant past, $r_* = \infty$ at $t = -\infty$, and reaches the horizon, $r_* = -\infty$, at $t = +\infty$. The radial in-fall problem is the easier to deal with, as the source term can be written in closed form. Zerilli used the symmetric normalization for the Fourier transform,

$$F(\omega) = (2\pi)^{-1/2} \int e^{i\omega t} f(t) dt \ ,$$

$$f(t) = (2\pi)^{-1/2} \int e^{-i\omega t} F(\omega) d\omega \ ,$$

and defined the source term [Zerilli,[12] Eq. (18)] without the minus sign. In the Laplace transforms used here the $1/(2\pi)$ is multiplied at the inverse transform, Eq. (7). The frequency-domain source, as given by Davis, Ruffini, Press, and Price[1] is, when multiplied by $-(2\pi)^{1/2}$ to match the convention used in this paper,

$$q^{(+)}(r, s_q) = -\frac{4(2\pi)^{1/2}(l+\frac{1}{2})^{1/2}(r-1)}{r(2\lambda r+3)} \times \left[r^{1/2} - \frac{4\lambda}{s_q(2\lambda r+3)} \right] e^{-s_q T(r)} \ , \tag{98}$$

where $\lambda \equiv \frac{1}{2}(l-1)(l+2)$, and $t = T(r)$ gives the time as a function of the radial coordinate along the geodesic followed by the particle:[40]

$$T(r) = -\tfrac{2}{3} r^{3/2} - 2r^{1/2} + \ln \left[\frac{r^{1/2}+1}{r^{1/2}-1} \right] . \tag{99}$$

The superscript $(+)$ indicates that the source is for the even-parity metric perturbations which satisfy the Zerilli equation

$$\frac{\partial^2}{\partial r_*^{\,2}} \psi^{(+)}(r_*, s) - [s^2 + V^{(+)}(r_*)] \psi^{(+)}(r_*, s) = -q^{(+)}(r_*, s) \ , \tag{100}$$

where $V^{(+)}$ is the Zerilli potential:[41]

$$V^{(+)} = \left[\frac{r-1}{r} \right] \frac{8\lambda^2(\lambda+1) r^3 + 12\lambda^2 r^2 + 18\lambda r + 9}{r^3(2\lambda r+3)^2} \ . \tag{101}$$

The homogeneous solutions $\psi^{(+)}(r_*, s)$ to Eq. (100) are given in terms of the corresponding homogeneous solutions to the Regge-Wheeler equation (1), with $m=2$, by Chandrasekhar:[42]

$$[2\lambda(\lambda+1) - 3s] \psi^{(+)}_{\rm hom}(r_*, s) = \left[2\lambda(\lambda+1) + \frac{9(r-1)}{r^2(2\lambda r+3)} \right] \psi_{\rm hom}(r_*, s) + 3\psi_{{\rm hom}, r_*}(r_*, s) \ . \tag{102}$$

The quasinormal mode function $\psi_q^{(+)}(r_*)$ is then found from Eqs. (26) and (102):

$$\psi_q^{(+)} = \left[1 + \frac{9(r-1)}{r^2(2\lambda r+3)[2\lambda(\lambda+1) - 3s_q]} \right] \psi_q + \frac{3(r-1)}{r^3[2\lambda(\lambda+1) - 3s_q]} \psi_{q,r} \ . \tag{103}$$

Simple algebra gives $\psi_q^{(+)}(r_*)$ in terms of the expansion coefficients a_n used in (26) for the odd-parity wave function $\psi(r_*)$:

$$\psi_q^{(+)} = \frac{(1-1/r)^{2s_q}}{\sum a_n(s_q)} \left[\left[1 + \frac{6s_q(2\lambda r+3) + 9(r-1)}{r^2(2\lambda r+3)[2\lambda(\lambda+1) - 3s_q]} \right] \sum_{n=0}^{\infty} a_n (1-1/r)^n + \frac{3(r-1)}{r^3[2\lambda(\lambda+1) - 3s_q]} \sum_{n=1}^{\infty} n a_n (1-1/r)^{n-1} \right] . \tag{104}$$

One last result, due to Chandrasekhar and Detweiler[43] and verifiable by inspection of Eq. (104), relates the transmission and reflection coefficients for the even-parity Zerilli wave functions to those for the odd-parity Regge-Wheeler wave functions:

$$T^{(+)}(s) = T(s) = A_{\rm in}^{-1}(s) \ , \tag{105}$$

$$R^{(+)}(s) = \frac{2\lambda(\lambda+1) - 3s}{2\lambda(\lambda+1) + 3s} R(s) \ , \tag{106}$$

which in turn implies

$$\alpha_q^{(+)} = \alpha_q \ , \tag{107}$$

$$A_{\rm out}^{(+)}(s_q) = \frac{2\lambda(\lambda+1) - 3s_q}{2\lambda(\lambda+1) + 3s_q} A_{\rm out}(s_q) \ . \tag{108}$$

Expressions (98) and (104)–(108) are then substituted into (92) to give the excitation coefficient $C_q^{(+)}$ for the even-parity perturbation:

$$C_q^{(+)} = \frac{A_{\rm out}^{(+)}(s_q)}{2s_q \alpha_q} \oint_{C_1} e^{-s_q r} \psi_q^{(+)}(r) q^{(+)}(r, s_q) \times (r-1)^{-s_q - 1} r \, dr \ . \tag{109}$$

The final contribution from the even-parity quasinormal modes is given by

$$\Psi_Q^{(+)}(r_*,t)=2\,\mathrm{Re}\left[\sum_{q=1}^{\infty} C_q^{(+)}\psi_q^{(+)}(r_*)e^{s_q(t-r_*)}\right]. \quad (110)$$

The $e^{-s_q T(r)}$ term in the $q^{(+)}(r)$ defined by Eq. (98) lets the integral (109) converge as $r\to\infty$ through real values, and the contour C_1 of Fig. 8(a) can be used if the end point is extended from $r=r_1$ to $r=\infty$. The result of integrating (109) on this contour was compared, for $q=1$, with integrating (97) on the real axis retaining only the $n=0$ term in Eq. (95) with $a=1$. Agreement was to within the truncation error of six decimal places.

For the purpose of comparison, the response function $\Psi(r_*,t)$ can, for large positive values of r_*, be generated by a Fourier transform of the single-particle wave amplitudes $A_l^{\mathrm{out}}(\omega)$ tabulated by Petrich, Shapiro, and Wasserman,[44]

$$\Psi(r_*,t)=(2\pi)^{-1/2}\int_{-\infty}^{\infty} A_l^{\mathrm{out}}(\omega)e^{-i\omega(t-r_*)}d\omega\,, \quad (111)$$

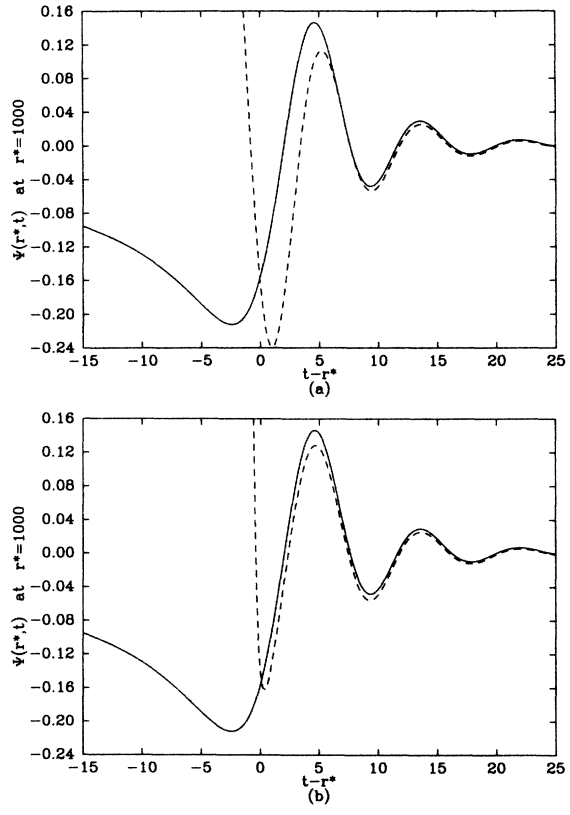

FIG. 10. Comparison of quasinormal ringing (dashed curve) with the total response (solid curve) for the $l=2$ radial in-fall problem. The solid curve was obtained from the Fourier coefficients tabulated by Petrich, Shapiro, and Wasserman (Ref. 44) and from those authors' Eq. (42). Specifically,

$$\Psi(r_*,t)=(2/\pi)^{1/2}\mathrm{Re}\left[\int_{\epsilon}^{1.9} A_l^{\mathrm{out}}(\omega)e^{i\omega(r_*-t)}d\omega\right].$$

The $A_l^{\mathrm{out}}(\omega)$ diverge as $\omega^{-1/3}$ as $\omega\to 0$, so that the smallest usable lower end point was $\epsilon=1\times10^{-8}$. Integration was done by NAg subroutine D01ANF. (a) shows the response from the first quasinormal mode; (b) shows the response from the first six.

and is the same as those authors' $R_l(r_*,t)$. Figure 10 compares $\Psi(r_*,t)$ as generated by Eq. (111) with the quasinormal mode expansion $\Psi_B(r_*,t)$ of Eq. (110). I tentatively assign the $\sim 10\%$ discrepancy in the time region $t-r_*\approx 5$ to inaccuracies in the Fourier coefficients: the excitation coefficients are probably accurate to at least five decimal places, and it is not likely that the branch-cut integral will contribute significantly at these times. Petrich, Shapiro, and Wasserman generate their wave functions by numerical integration of the homogeneous Zerilli equation. More accurate low-frequency results might be obtained using the algorithm for $\psi^{(+)}(r,s)$ discussed here: expression (104) can be used at arbitrary complex s provided sufficient precision is used when generating the expansion coefficients (see Appendix A). As in the case of the initial- and characteristic-value problems, the branch-cut contribution Ψ_B will cause the radiation generated by small body in-fall to be characterized at late times by a radiative decay tail. The analysis is difficult, however, and must await more detailed study.

VI. CONCLUSION

Analytic representations for generalized spheroidal wave functions have been used to evaluate the important low-frequency components of the radiative Green's function that propagates small perturbations to the Schwarzschild geometry. Quasinormal mode decompositions have been demonstrated for several important classes of astrophysical problems, and a new type of radiation effect discovered in the form of radiating decay tails. This study is among the first in which a direct comparison has been made between independent means of propagating source functions, and indicates that the analytic representation can yield useful and accurate results for problems, such as that of in-falling bodies, or any problem involving the Kerr geometry, where direct numerical integration of the wave equation is difficult.[46]

ACKNOWLEDGMENTS

Thanks are due Calvin H. Wilcox for insight into Laplace transforms and the initial-value problem. This study was suggested by Richard H. Price, who provided many useful discussions on Green's functions, in-fall, and stellar collapse. Crucial questions concerning branch cuts and poles could be addressed only through recourse to extensive and difficult numerical experimentation, and none of the analysis presented in this paper would have been possible without the assistance and professional expertise of the operations staff of the University of Utah College of Computer Science. Sincerest thanks are due Pieter Bowman, Arlen Duncan, Alan Lichty, Lon Willet, Douglas Hendry, and Nelson H. F. Beebe. Computational facilities were made available by the Department of Physics, the College of Science Computer, and the Center for Computer Aided Geometric Design.

APPENDIX A: SOME COMPUTATIONAL DETAILS

The response of black-hole geometries to small perturbations is dominated at all but late times by quasinormal

ringing. Although one result of this paper is the demonstration that some small amount of the stress-energy associated with the perturbation will be carried off through the branch-cut mechanism of the radiative decay tail, most of this energy may be expected to be radiated away through the quasinormal modes. This radiative form is seen explicitly in expression (27) for the quasinormal mode contribution I_Q to the radiative Green's function G:

$$G_Q(r_*,t\mid r'_*,t') = 2\,\mathrm{Re}\left[\sum_{q=1}^{\infty}\frac{\psi_q(r_*)\psi_q(r'_*)e^{s_q(t-t'-r_*-r'_*)}}{2s_q\alpha_q A_{\mathrm{out}}{}^{-1}(s_q)}\right]. \tag{A1}$$

As a formal expression, (A1) is comfortably elegant. It is of no computational utility, however, unless one can compute the quasinormal frequencies s_q, the quasinormal mode functions $\psi_q(r)$, and the derivatives α_q of the amplitude $A_{\mathrm{in}}(s)$.

1. Quasinormal frequencies, quasinormal modes, and the function $\psi_{r_+}(r_*,s)$

Accurate values for the underdamped Schwarzschild gravitational quasinormal frequencies, for which $|\mathrm{Re}(s_q)| < |\mathrm{Im}(s_q)|$, were first obtained by Chandrasekar and Detweiler.[14] Corresponding values for underdamped scalar and electromagnetic frequencies were given by Cunningham, Price, and Moncrief.[16] The present method of calculation, which gives values for the overdamped as well as the underdamped frequencies, is outlined as follows (see paper I for details).

The quasinormal mode functions $\psi_q(r_*)$ are generated from expression (26),

$$\psi_q(r_*) = (1-r^{-1})^{2s_q}\frac{\sum_{n=0}^{\infty}a_n(s_q)(1-r^{-1})^n}{\sum_{n=0}^{\infty}a_n(s_q)}. \tag{A2}$$

The expansion coefficients a_n form the minimal solution to the recurrence relation:

$$\begin{aligned}&\alpha_0 a_1+\beta_0 a_0=0\,,\\ &\alpha_n a_{n+1}+\beta_n a_n+\gamma_n a_{n-1}=0,\quad n=1,2,\ldots,\end{aligned} \tag{A3}$$

where the recurrence coefficients α_n, β_n, and γ_n are given by

$$\begin{aligned}\alpha_n &= n^2+(2s+2)n+2s+1\,,\\ \beta_n &= -[2n^2+(8s+2)n+8s^2+4s+l(l+1)\\ &\quad -m^2+1]\,,\\ \gamma_n &= n^2+4sn+4s^2-m^2\,,\end{aligned} \tag{A4}$$

and may be generated by downward recursion from suitably large n. Note the α_n, β_n, and γ_n are real when s is real, so that $a_n(\bar{s})=\bar{a}_n(s)$. Computational aspects of three-term recurrence relations are discussed by Gautschi.[45]

The coefficients are normalized so that $a_0\equiv 1$. Care must be taken since the largest of the a_n is not a_0, but rather a_q, which may be several orders of magnitude larger than a_0. A short upward recursion from a_0 to a_q is frequently necessary to accurately generate a_1 through a_{q-1}. The quasinormal frequency s_q (or $\bar{s}_q$) is the qth root (or its complex conjugate) of the continued-fraction equation

$$0=\beta_0-\cfrac{\alpha_0\gamma_1}{\beta_1-\cfrac{\alpha_1\gamma_2}{\beta_2-\cfrac{\alpha_2\gamma_3}{\beta_3-\cdots}}}. \tag{A5}$$

The function $\psi_{r_+}(r,s)$ can be generated from Eq. (17) using expansion coefficients $a_n(s)$ generated from the recurrence relation (A3). If s is not a quasinormal frequency s_q or $\bar{s}_q$, then the a_n are dominant and must be generated by forward recursion starting from $a_0=1$. When s is a quasinormal frequency the a_n are minimal and should be generated by downward recursion.

2. The ingoing and outgoing functions $\psi_{\infty_-}(r,s)$ and $\psi_{\infty_+}(r,s)$

The amplitudes $A_{\mathrm{in}}(s)$ and $A_{\mathrm{out}}(s)$ are calculated by matching the solutions that are ingoing and outgoing as $r\to\infty$, respectively, $\psi_{\infty_-}(r,s)$ and $\psi_{\infty_+}(r,s)$, to the event horizon solution $\psi_{r_+}(r,s)$. Accurate determination of the derivative α_q requires precise values of $A_{\mathrm{in}}(s)$ in the immediate neighborhood of the quasinormal frequencies. Detweiler[47] describes a numerical solution for $A_{\mathrm{in}}(s)$ near the fundamental resonance s_1. His method, however, interpolates the zero s_1 of $A_{\mathrm{in}}(s)$ from nearby values of A_{in} on the imaginary s axis, where the values of the functions ψ_{∞_-}, ψ_{∞_+}, and ψ_{r_+} can be obtained with reasonable accuracy through numerical integration of the homogeneous form of Eq. (8). This approach might be accurate enough to give α_1 to a few decimal places. Accurate numerical integration of y_+ and y_- for complex s is difficult and is discussed by Press and Teukolsky.[48] Although it is conceivable that Press and Teukolsky's integration technique might be capable of extending Detweiler's method to other underdamped resonances, it is unlikely that any numerical integration method will readily give values of $A_{\mathrm{in}}(s)$ at overdamped frequencies with sufficient accuracy to allow a reliable calculation of the relevant α_q. Without reliable values for these α_q it will not be possible to determine the convergence and completeness properties of the quasinormal mode expansion (A1).

The present calculation of A_{in} and A_{out} uses the analytic definition for the functions ψ_{∞_-} and ψ_{∞_+} given by Eqs. (18) and (19):

$$\psi_{\infty\pm}(r,s)=(2is)^{\pm s}e^{\pm i\phi_\pm}(1-r^{-1})^s \times \sum_{L=-\infty}^{\infty} b_L[G_{L+\nu}(\eta,\rho)\pm iF_{L+\nu}(\eta,\rho)] . \quad \text{(A6)}$$

The normalization phases ϕ_+ and ϕ_- are given by Eq. (19), and the expansion coefficients b_L are the solution, minimal as $L\to\pm\infty$, of the three-term recurrence relation

$$\alpha_L b_{L+1}+\beta_L b_L+\gamma_L b_{L-1}=0 . \quad \text{(A7)}$$

The recursion coefficients α_L, β_L, and γ_L are given by

$$\begin{aligned}
\alpha_L &= -\frac{isR_{L+1}}{2L+2\nu+3}[(L+\nu+1)(L+\nu+2)-(L+\nu+2)(2s+1)-m^2+(s+1)^2] ,\\
\beta_L &= (L+\nu)(L+\nu+1)+3s^2-l(l+1)+isQ_L[(L+\nu)(L+\nu+1)-m^2+s^2] ,\\
\gamma_L &= -\frac{isR_L}{2L+2\nu-1}[(L+\nu)(L+\nu-1)+(L+\nu-1)(2s+1)-m^2+(s+1)^2] ,
\end{aligned} \quad \text{(A8)}$$

where

$$Q_L=\frac{\eta}{(L+\nu)(L+\nu+1)}$$

and (A9)

$$R_L=\frac{[(L+\nu)^2+\eta^2]^{1/2}}{L+\nu} .$$

The recurrence is always ended at $L=0$, with $b_0\equiv 1$. The phase parameter ν is that solution of the implicit continued-fraction equation

$$\beta_0=\cfrac{\alpha_{-1}\gamma_0}{\beta_{-1}-\cfrac{\alpha_{-2}\gamma_{-1}}{\beta_{-2}-\cfrac{\alpha_{-3}\gamma_{-2}}{\beta_{-3}-\cdots}}}+\cfrac{\alpha_0\gamma_1}{\beta_1-\cfrac{\alpha_1\gamma_2}{\beta_2-\cfrac{\alpha_2\gamma_3}{\beta_3-\cdots}}} , \quad \text{(A10)}$$

that goes to l as $s\to 0$. It is frequently difficult to find solutions for ν when $|s|$ is large, and the highest-order mode for which I have thus far been able to accurately calculate α_q is for $q=7$. Despite this shortcoming, the computer program that generates the solutions y_+ and y_- is quite general, and will eventually be published. Further details of the algorithm are discussed in paper II.

3. The amplitudes $A_{in}(s)$ and $A_{out}(s)$, and the derivative α_q

The amplitudes A_{in} and A_{out} are defined, as functions of s, to be solutions of

$$\begin{aligned}
\psi_{r_+}(r,s) &= A_{in}\psi_{\infty_+}(r,s)+A_{out}\psi_{\infty_-}(r,s) ,\\
\psi_{r_+,r}(r,s) &= A_{in}\psi_{\infty_+,r}(r,s)+A_{out}\psi_{\infty_-,r}(r,s) .
\end{aligned} \quad \text{(A11)}$$

The computer program that generates the Coulomb wave functions used in expansion (A6) gives most accurate results for values of $\rho=isr$ that lie in the fourth quadrant near the real ρ axis. The choice of the r value at which the system (A11) was solved for A_{in} was determined by this condition, and the requirement that $|1-r^{-1}|<1$ [otherwise series (26) will not converge]. The amplitude $A_{in}(s)$ is zero when s is a quasinormal frequency s_q. The derivatives

$$\alpha_q\equiv\frac{d}{ds}A_{in}(s)\bigg|_{s=s_q} ,$$

were found by Lagrangian interpolation[49] from values of $A_{in}(s)$ near $s=s_q$. Values for the α_q are listed in Table I. The number of significant digits listed is the number of places to which A_{in} was zero, and to which the Cauchy-Riemann analyticity condition was satisfied by the derivative.

4. A note on integration

The problem of integrating source terms $q(r,s)$ over the ingoing wave function $\psi_{r_+}(r,s)$ is a general one that arises when evaluating the branch-cut integrals Ψ_B of Sec. III and the Fourier coefficients $A_l^{out}(\omega)$ of Sec. V, in addition to computing the excitation coefficients C_q that are the major concern of the present work. Very low frequencies pose a particular problem. The contour techniques used

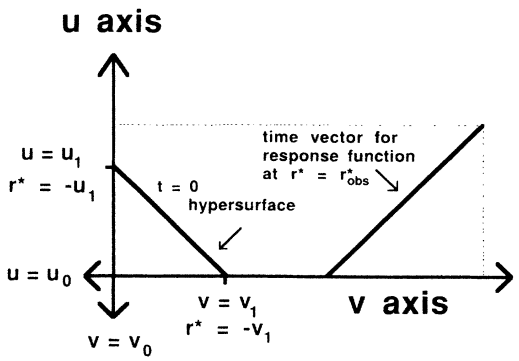

FIG. 11. Spacetime diagram of the characteristic-value problem in characteristic (u,v) coordinates.

for computing the C_q are, however, readily generalizable. Consider the problem of computing the Fourier coefficient $A_l^{\text{out}}(s)$ as a general function of the frequency $s=-i\omega$:

$$A_l^{\text{out}}(s)=-(2\pi)^{-1/2}\int_1^\infty \psi_{r_+}(r,s)q(r,s)(r-1)^{-1}r\,dr\ . \tag{A12}$$

The integral usually converges on the real r axis when $s=-i\omega$ is purely imaginary, but the convergence is not absolute. However, the convergence can be made absolute if $\psi^{(+)}(r,s)$ is decomposed into ingoing and outgoing components after some mediocre value $r=r_1$, and the two resulting integrals finished with $\text{Im}(r)\to\pm\infty$. Assume $\omega=is>0$. Then

$$\begin{aligned}A_l^{\text{out}}(s)=&-(2\pi)^{-1/2}\int_1^{r_1}\psi_{r_+}(r,s)q(r,s)(r-1)^{-1}r\,dr-(2\pi)^{-1/2}A_{\text{in}}(s)\int_{r_1}^{-i\infty}\psi_{\infty_-}(r,s)q(r,s)(r-1)^{-1}r\,dr\\&-(2\pi)^{-1/2}A_{\text{out}}(s)\int_{r_1}^{+i\infty}\psi_{\infty_+}(r,s)q(r-1)^{-1}r\,dr\ .\end{aligned} \tag{A13}$$

As we have seen, the decomposition $\psi_{r_+}=A_{\text{in}}\psi_{\infty_-}+A_{\text{out}}\psi_{\infty_+}$ can be done quite accurately, and the form of (A13) was used in the investigations of the small s behavior of the branch-cut integrals. Use of integration contour C_1 of Fig. 8 will frequently be necessary for the first integral when the integrand diverges as $r\to 1$.

APPENDIX B: GREEN'S-FUNCTION PROPAGATION OF CHARACTERISTIC DATA

We desire an expression relating the response $\Psi(r_*,t)$ due to data specified on the null rays $t-r_*=u_0$ and $t+r_*=v_0$. The problem is diagramed in Fig. 11. For the moment ignore the $t=0$ hypersurface, and assume we wish to integrate the response function $\Psi(u,v)$ in the entire rectangular region indicated, given the value of Ψ and its derivatives on the $u=u_0$ and $v=v_0$ boundary characteristics. The derivation of the desired expression is similar to that for the response from initial data, Eq. (4), which is discussed by Morse and Feshbach.[50] We start with Eqs. (1) and (2):

$$\frac{\partial^2}{\partial r_*^{\,2}}\Psi(r_*,t)-\frac{\partial^2}{\partial t^2}\Psi(r_*,t)-V(r_*)\Psi(r_*,t)=-Q(r_*,t)\ , \tag{B1}$$

$$\begin{aligned}&\frac{\partial^2}{\partial r_*^{\,2}}G(r_*,t\mid r'_*,t')-\frac{\partial^2}{\partial t^2}G(r_*,t\mid r'_*,t')\\&\qquad-V(r_*)G(r_*,t\mid r'_*,t')=-\delta(r_*-r'_*)\delta(t-t')\ .\end{aligned} \tag{B2}$$

In terms of the characteristic coordinates $u'=t'-r'_*$ and $v'=t'+r'_*$, these equations can be written

$$\Psi_{,u'v'}(u',v')+\tfrac{1}{4}V(v'-u')\Psi(u',v')=\tfrac{1}{4}Q(u',v')\ , \tag{B3}$$

$$\begin{aligned}&G_{,u'v'}(u,v\mid u',v')+\tfrac{1}{4}V(u'-v')G(u,v\mid u',v')\\&\qquad=\delta(u-u'-v+v')\delta(u-u'+v-v')\ .\end{aligned} \tag{B4}$$

Multiply the first of these by G, the second by Ψ, subtract the two, and integrate the difference:

$$\begin{aligned}&\int_{u'=u_0}^\infty\int_{v'=v_0}^\infty[G(u,v\mid u',v')\Psi_{,u'v'}(u',v')-G_{,u'v'}(u,v\mid u',v')\Psi(u',v')]du'dv'\\&\qquad=\tfrac{1}{4}\int_{u'=u_0}^\infty\int_{v'=v_0}^\infty G(u,v\mid u',v')Q(u',v')du'dv'\\&\qquad\quad-\int_{u'=u_0}^\infty\int_{v'=v_0}^\infty\Psi(u',v')\delta[(u-u')-(v-v')]\delta[(u-u')+(v-v')]du'dv'\ .\end{aligned} \tag{B5}$$

The double integral on the left-hand side of the equation may be expressed as a sum of differentials, and the δ functions on the right-hand side integrated out:

$$\begin{aligned}&\kappa\int_{u'=u_0}^\infty\int_{v'=v_0}^\infty\{[G(u,v\mid u',v')\Psi_{,u'}(u',v')]_{,v'}-[G_{,v'}(u,v\mid u',v')\Psi(u',v')]_{,u'}\}du'dv'\\&\quad+(1-\kappa)\int_{u'=u_0}^\infty\int_{v'=v_0}^\infty\{[G(u,v\mid u',v')\Psi_{,v'}(u',v')]_{,u'}-[G_{,u'}(u,v\mid u',v')\Psi(u',v')]_{,v'}\}du'dv'\\&\qquad=\tfrac{1}{4}\int_{u'=u_0}^\infty\int_{v'=v_0}^\infty G(u,v\mid u',v')Q(u',v')du'dv'-\tfrac{1}{2}\Psi(u,v)\ .\end{aligned} \tag{B6}$$

Here κ is a constant that may take any complex value, although 0, $\frac{1}{2}$, and 1 will probably prove the most useful. The values $u'=\infty$ and $v'=\infty$ correspond to $t=\infty$, and causality requires that the contribution at these end points vanish. Equation (B6) is then rearranged to yield

$$\Psi(u,v)=2\kappa\left[\int_{u_0}^{\infty}G(u,v\mid u',v_0)\Psi_{,u'}(u',v_0)du'-\int_{v_0}^{\infty}G_{,v'}(u,v\mid u_0,v')\Psi(u_0,v')dv'\right]$$
$$+2(1-\kappa)\left[\int_{v_0}^{\infty}G(u,v\mid u_0,v')\Psi_{,v'}(u_0,v')dv'-\int_{u_0}^{\infty}G_{,u'}(u,v\mid u',v_0)\Psi(u',v_0)du'\right]$$
$$+\tfrac{1}{2}\int_{u_0}^{\infty}\int_{v_0}^{\infty}G(u,v\mid u',v')Q(u',v')du'dv' . \tag{B7}$$

This expression should be compared with Eq. (4). The factor $\frac{1}{2}$ appears in the last integral because of the form the δ functions take in the (u,v) definition of G, Eq. (B4). An expression for the response function $\Psi(r_*,t)$ for the mixed Cauchy and characteristic data problem, where the triangular region bounded by the $u=u_0$ and $v=v_0$ axis and the $t=0$ hypersurface is to be excluded from the lower left corner of Fig. 11, is obtained by superposition of Eqs. (B7) and (4):

$$\Psi(r_*,t)=2\kappa\left[\int_{u_1}^{\infty}G(u,v\mid u',v_0)\Psi_{,u'}(u',v_0)du'-\int_{v_1}^{\infty}G_{,v'}(u,v\mid u_0,v')\Psi(u_0,v')dv'\right]$$
$$+2(1-\kappa)\left[\int_{v_1}^{\infty}G(u,v\mid u_0,v')\Psi_{,v'}(u_0,v')dv'-\int_{u_1}^{\infty}G_{,u'}(u,v\mid u',v_0)\Psi(u',v_0)du'\right]$$
$$+\int_{-u_1}^{v_1}[G(r_*,t\mid r'_*,t')\Psi_{,t'}(r'_*,t')-\Psi(r'_*,t')G_{,t'}(r_*,t\mid r'_*,t')]_{t'=t_0}dr'_*$$
$$+\int_0^{\infty}\int_{-\infty}^{\infty}G(r_*,t\mid r'_*,t')Q(r'_*,t')dr'_*dt' . \tag{B8}$$

Further integrations by parts will sometimes be useful.

---

*Present address: The BDM Corporation, 1801 Randolph Road, S.E., Albuquerque, NM 87106.

[1]M. Davis, R. Ruffini, W. H. Press, and R. H. Price, Phys. Rev. Lett. **27**, 1466 (1971).

[2]M. Davis, R. Ruffini, and J. Tiomno, Phys. Rev. D **5**, 2932 (1972).

[3]S. Detweiler, Proc. R. Soc. London **A352**, 381 (1977).

[4]S. Detweiler, in *Sources of Gravitational Radiation*, edited by L. Smarr (Cambridge University Press, New York, 1979), p. 211.

[5]S. Detweiler and E. Szedenits, Astrophys. J. **231**, 211 (1979).

[6]E. W. Leaver, Proc. R. Soc. London **A402**, 285 (1985), paper I.

[7]E. W. Leaver, J. Math. Phys. **27**, 1238 (1986), paper II.

[8]S. Detweiler and R. Ove, Phys. Rev. Lett. **51**, 67 (1983).

[9]C. W. Misner, K. S. Thorne, and J. A. Wheeler, *Gravitation* (Freeman, San Francisco, 1973), exercise 32.10.

[10]J. A. Wheeler, Phys. Rev. **97**, 511 (1955).

[11]T. Regge and J. A. Wheeler, Phys. Rev. **108**, 1063 (1957).

[12]F. J. Zerilli, Phys. Rev. D **2**, 2141 (1970).

[13]S. Chandrasekhar, Proc. R. Soc. London **A343**, 289 (1975).

[14]S. Chandrasekhar and S. Detweiler, Proc. R. Soc. London **A344**, 441 (1975).

[15]R. H. Price, Phys. Rev. D **5**, 2419 (1972).

[16]C. T. Cunningham, R. H. Price, and V. Moncrief, Astrophys. J. **224**, 643 (1978).

[17]C. T. Cunningham, R. H. Price, and V. Moncrief, Astrophys. J. **230**, 870 (1979).

[18]C. T. Cunningham, R. H. Price, and V. Moncrief, Astrophys. J. **236**, 674 (1980).

[19]V. Moncrief, C. T. Cunningham, and R. H. Price, in *Sources of Gravitational Radiation*, edited by L. Smarr (Cambridge University Press, New York, 1979), p. 231.

[20]L. I. Petrich, S. L. Shapiro, and I. Wasserman, Astrophys. J. Suppl. Ser. **58**, 297 (1985).

[21]P. M. Morse and H. Feshbach, *Methods of Theoretical Physics* (McGraw-Hill, New York, 1953), Eq. (7.3.5). All present Green's-function derivations were adapted from material in this chapter.

[22]The concept of eigensolutions to the homogeneous Regge-Wheeler equation satisfying boundary conditions that the wave behavior be purely ingoing at the horizon and purely outgoing at spatial infinity appears to have originated with Vishveshwara, who also recognized the corresponding eigenfrequencies as being poles of the scattering matrix: see C. V. Vishveshwara, Phys. Rev. D **1**, 2870 (1970), especially p. 2879. The term *quasinormal mode* was applied by Press (Ref. 25).

[23]Detweiler (Ref. 3), Eq. (36).

[24]C. V. Vishveshwara, Nature **227**, 936 (1970).

[25]W. Press, Astrophys. J. **170**, L105 (1971).

[26]L. Smarr, in *Sources of Gravitational Radiation* (Ref. 19), p. 245.

[27]I. S. Gradshteyn and I. M. Ryzhik, *Table of Integrals, Series, and Products* (Academic, New York, 1965).

[28]Morse and Feshbach (Ref. 21), p. 837.

[29]Three of these regions have been previously identified by Davis, Ruffini, and Tiomno (Ref. 2).

[30]Morse and Feshbach (Ref. 21), p. 612.

[31]L. J. Slater, in *Handbook of Mathematical Functions*, edited by M. Abramowitz and I. Stegun (National Bureau of Standards, Washington, D.C., 1964), Chap. 13.

[32]Expression (64) is a generalization of a result originally obtained by R. H. Price (private communication), who in a similar consideration of the initial-value problem kept r real and, the integral then being convergent only for $\mathrm{Re}(s)>0$, performed an analytic continuation argument on the frequency parameter s. Although the two approaches must be equivalent, the present contour method of solution has, in practice, thus far proved the more powerful.

[33]H. Kuki, Commun. ACM **15**, 262 (1972).

[34]Cunningham, Price, and Moncrief (Refs. 16–18). In particular, the hypergeometric function expression for the initial exterior perturbation field arising from stellar collapse, Eq. (III.6) of Ref. 16, can be expressed in this form.

[35]Cunningham, Price, and Moncrief (Ref. 16), Eq. (III.12).

[36]Misner, Thorne, and Wheeler (Ref. 9), p. 851.

[37]Moncrief, Cunningham, and Price (Ref. 19). The dashed curve in Fig. 1 of this paper is the same as the $r_0=8M$ curve in Fig. 5(c) of Ref. 16, but with the abscissa scaled (as in the present reproduction) in terms of the magnitude q_l of the initial perturbation.

[38]Y. L. Luke, *Algorithms for the Computation of Mathematical Functions* (Academic, New York, 1977).

[39]The integrals were evaluated numerically using Numerical Algorithm Group (NAg) adaptive quadrature routine D01APF. The equivalence of these two integrals can also be demonstrated analytically, and having two different expressions for the same quantity was useful when developing the computer code. Figures 2, 4, 5, 7, 9, and 10 were prepared with the ⟨PLOT79⟩ graphics system, which was very useful in deducing the behavior of the response functions. All programs were either TOPS-20 or VAX/VMS FORTRAN.

[40]Misner, Thorne, and Wheeler (Ref. 9), Eq. (25.38). The geodesic $T(r)$ given by Davis *et al.* (Refs. 1 and 2) should be multiplied by a factor of M.

[41]S. Chandrasekhar, *The Mathematical Theory of Black Holes* (Clarendon Press, Oxford, 1983), Chap. 4, Eq. (63) with $2M=1$.

[42]Chandrasekhar (Ref. 41), Chap. 4, Eq. (152) with $\sigma=is$ and $2\mu^2=\lambda$. Also see Ref. 14.

[43]Chandrasekhar and Detweiler (Ref. 14). This result is also derived in Ref. 41, Chap. 4, Eq. (167).

[44]Petrich, Shapiro, and Wasserman (Ref. 20). These authors retain the identical Zerilli-based formalism as Davis, Ruffini, Press, Price, and Tiomno (Refs. 1 and 2), while Detweiler and Szedenits (Ref. 5) compute metric perturbations in terms of the gauge-invariant Newman-Penrose quantity ψ_4. This last approach can be generalized to rotating black holes. The most efficient single-body in-fall mechanism for generating gravitational radiation probably involves binary systems of a neutron star in a decaying orbit around a black hole, and the black hole will have appreciable angular momentum after the final collision. Generalization of the present perturbation results to the Kerr geometry would appear desirable in analysis of cases where the mass of the black hole differs from that of the neutron star by a factor of more than ~ 5.

[45]W. Gautschi, SIAM Rev. **9**, 24 (1967).

[46]Related developments in the analytic theory of solutions to the spin-zero Regge-Wheeler equation are discussed by P. Candelas and K. W. Howard, Phys. Rev. D **29**, 1618 (1984); K. W. Howard, *ibid.* **30**, 2532 (1984); B. P. Jensen and P. Candelas, *ibid.* **33**, 1590 (1986). I thank B. Whiting for bringing these references to my attention while the present paper was in review.

[47]S. Detweiler, Astrophys. J. **239**, 292 (1980).

[48]W. Press and S. Teukolsky, Astrophys. J. **185**, 649 (1971).

[49]P. J. Davis and I. Polonsky, in *Handbook of Mathematical Functions* (Ref. 31), Eq. (25.3.6) with $h\sim 0.001$.

[50]Morse and Feshbach (Ref. 21), pp. 834–837.